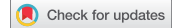


RESEARCH PAPER



SQSTM1/p62 and PPARGC1A/PGC-1alpha at the interface of autophagy and vascular senescence

Gloria Salazar^{a,b}, Abigail Cullen^a, Jingwen Huang^a, Yitong Zhao^c, Alexa Serino^a, Lula Hilenski^d, Nikolay Patrushev^{id}, Farshad Forouzandeh^e, and Hyun Seok Hwang^a

^aDepartment of Nutrition, Food and Exercise Sciences, Florida State University, Tallahassee, FL, USA; ^bCenter for Advancing Exercise and Nutrition Research on Aging (CAENRA), Florida State University, Tallahassee, FL, USA; ^cDivision of Nephrology and Hypertension, Department of Medicine, University of California, Irvine, CA, USA; ^dDepartment of Medicine, Division of Cardiology, Emory University, Atlanta, GA, USA; ^eDepartment of Medicine, Case Western Reserve University School of Medicine and Harrington Heart and Vascular Institute, Cleveland, OH, USA

ABSTRACT

Defective macroautophagy/autophagy and mitochondrial dysfunction are known to stimulate senescence. The mitochondrial regulator PPARGC1A (peroxisome proliferator activated receptor gamma, coactivator 1 alpha) regulates mitochondrial biogenesis, reducing senescence of vascular smooth muscle cells (VSMCs); however, it is unknown whether autophagy mediates PPARGC1A-protective effects on senescence. Using *ppargc1a*^{-/-} VSMCs, we identified the autophagy receptor SQSTM1/p62 (sequestosome 1) as a major regulator of autophagy and senescence of VSMCs. Abnormal autophagosomes were observed in VSMCs in aortas of *ppargc1a*^{-/-} mice. *ppargc1a*^{-/-} VSMCs in culture presented reductions in LC3-II levels; in autophagosome number; and in the expression of SQSTM1 (protein and mRNA), LAMP2 (lysosomal-associated membrane protein 2), CTSD (cathepsin D), and TFRC (transferrin receptor). Reduced SQSTM1 protein expression was also observed in aortas of *ppargc1a*^{-/-} mice and was upregulated by PPARGC1A overexpression, suggesting that SQSTM1 is a direct target of PPARGC1A. Inhibition of autophagy by 3-MA (3-methyladenine), spautin-1 or *Atg5* (autophagy related 5) siRNA stimulated senescence. Rapamycin rescued the effect of *Atg5* siRNA in *Ppargc1a*^{+/+}, but not in *ppargc1a*^{-/-} VSMCs, suggesting that other targets of MTOR (mechanistic target of rapamycin kinase), in addition to autophagy, also contribute to senescence. *Sqstm1* siRNA increased senescence basally and in response to AGT II (angiotensin II) and zinc overload, two known inducers of senescence. Furthermore, *Sqstm1* gene deficiency mimicked the phenotype of *Ppargc1a* depletion by presenting reduced autophagy and increased senescence *in vitro* and *in vivo*. Thus, PPARGC1A upregulates autophagy reducing senescence by a SQSTM1-dependent mechanism. We propose SQSTM1 as a novel target in therapeutic interventions reducing senescence.

Abbreviations: 3-MA: 3-methyladenine; ACTA2/SM-actin: actin, alpha 2, smooth muscle, aorta; ACTB/ β -actin: actin beta; AGT II: angiotensin II; ATG5: autophagy related 5; BECN1: beclin 1; CAT: catalase; CDKN1A: cyclin-dependent kinase inhibitor 1A (P21); Chl: chloroquine; CTSD: cathepsin D; CYCS: cytochrome C, somatic; DHE: dihydroethidium; DPBS: Dulbecco's phosphate-buffered saline; EL: elastic lamina; EM: extracellular matrix; FDG: fluorescein-di- β -D-galactopyranoside; GAPDH: glyceraldehyde-3-phosphate dehydrogenase; γ H2AFX: phosphorylated H2A histone family, member X, H₂DCFDA: 2',7'-dichlorodihydrofluorescein diacetate; LAMP2: lysosomal-associated membrane protein 2; MASMs: mouse vascular smooth muscle cells; MEF: mouse embryonic fibroblast; NBR1: NBR1, autophagy cargo receptor; NF κ B/NF- κ B: nuclear factor of kappa light polypeptide gene enhancer in B cells; MTOR: mechanistic target of rapamycin kinase; NFE2L2: nuclear factor, erythroid derived 2, like 2; NOX1: NADPH oxidase 1; OPTN: optineurin; PFA: paraformaldehyde; PFU: plaque-forming units; PPARGC1A/PGC-1 α : peroxisome proliferator activated receptor, gamma, coactivator 1 alpha; PtdIn3K: phosphatidylinositol 3-kinase; RASMs: rat vascular smooth muscle cells; ROS: reactive oxygen species; SA-GLB1/ β -gal: senescence-associated galactosidase, beta 1; SASP: senescence-associated secretory phenotype; SIRT1: sirtuin 1; Spautin 1: specific and potent autophagy inhibitor 1; SQSTM1/p62: sequestosome 1; SOD: superoxide dismutase; TEM: transmission electron microscopy; TFEB: transcription factor EB; TFRC: transferrin receptor; TRP53/p53: transformation related protein 53; TUBG1: tubulin gamma 1; VSMCs: vascular smooth muscle cells; WT: wild type

ARTICLE HISTORY

Received 9 August 2018
Revised 7 August 2019
Accepted 9 August 2019

KEYWORDS

Aging; autophagy; oxidative stress; senescence; SQSTM1; vascular biology

Introduction

Mitochondrial function and autophagy, two critical processes involved in protection against oxidative stress, decline with age [1,2]. Increased mitochondrial dysfunction during aging,

in part by decreased biogenesis, promotes oxidative stress that causes damage to DNA, proteins and lipids, and is a major inducer of vascular senescence. Expression of mitochondrial electron transport chain components decreases with age [3],

CONTACT Gloria Salazar ✉ gsalazar@fsu.edu Department of Nutrition, Food and Exercise Sciences, Florida State University, 120 Convocation Way, Sandels Building Suite 408, Tallahassee, FL 32306, USA

 Supplemental data for this article can be accessed [here](#).

© 2019 Informa UK Limited, trading as Taylor & Francis Group

as does PPARGC1A [4], a central organizer of metabolic function, oxidative states, and mitochondrial biogenesis and function [5]. The PPARGC1 family of transcriptional co-activators (PPARGC1A, PPARGC1B and PPRC1) induces a robust upregulation of transcriptional activity and mitochondrial function [5]. PPARGC1A, the best-studied member of this family, controls mitochondrial biogenesis by co-activating major transcription factors regulating mitochondrial genes, including NFE2L2 (nuclear factor, erythroid derived 2, like 2) [5]. We reported a novel function for PPARGC1A as a negative regulator of vascular senescence [6], a process that was associated with increased oxidative stress, telomere dysfunction and atherosclerosis [7]. However, little is known about the contribution of PPARGC1A to autophagy and the role of defective autophagy in senescence induced by *Ppargc1a* gene deficiency.

Autophagy is a process that mediates the degradation of cytoplasmic components, such as dysfunctional mitochondria (mitophagy) [8] and protein aggregates, through lysosome-mediated degradation, thus promoting cellular homeostasis [9]. Autophagy has also been associated with reduced senescence. In primary human fibroblasts, depletion of *Atg12*, *Atg7* or *Lamp2* causes senescence, which is associated with increased levels of reactive oxygen species (ROS) and reduced expression of autophagy genes, including SQSTM1 [10]. Interestingly, both replicative senescence and senescence induced by defective autophagy correlated with reduced SQSTM1 protein levels [10]. Similarly, in fibroblasts, senescence induced by oxidative stress was mediated by defective autophagy caused by lysosomal dysfunction [11]. In the cardiovascular system, defective autophagy by *Atg7* depletion led to the accumulation of SQSTM1 and senescence of VSMCs, and to diet-induced atherosclerosis [12]. SQSTM1 is an autophagy receptor involved in the targeting of cargo into autophagosomes. After the fusion of autophagosomes with lysosomes, the autophagosome content including SQSTM1 is degraded [13]. Thus, SQSTM1 protein levels have been used as an indicator of autophagic flux.

TFEB (transcription factor EB) is a master regulator of lysosomal biogenesis [14] and autophagy [15]. PPARGC1A and TFEB co-regulate each other, as seen in mouse embryonic fibroblasts [16], suggesting that PPARGC1A may regulate autophagy through a TFEB-dependent mechanism; however, evidence of the direct role of PPARGC1A in promoting autophagy and the possible mechanism involved are lacking.

sqstm1^{-/-} mice present increased mitochondrial oxidative stress, decreased lifespan [17], mature-onset obesity, and insulin resistance [18]. *Sqstm1* depletion was also shown to increase atherosclerosis in *apoe*^{-/-} mice fed high fat diet [19]. It is unknown, however, whether PPARGC1A and SQSTM1 functionally interact to regulate autophagy and cellular senescence. Here, we demonstrated that PPARGC1A regulates autophagy and SQSTM1 expression and that SQSTM1 downregulation mediates PPARGC1A deficiency-induced senescence.

Results

Using an *apoe*^{-/-} *ppargc1a*^{-/-} animal model, we previously demonstrated that PPARGC1A is a negative regulator of

vascular senescence [6]. Increased vascular senescence in this animal model is associated with accelerated deposition of plaque in the aorta, DNA damage and telomere shortening [7]. However, it is unknown whether defective autophagy contributes to these effects. To assess signs of dysfunctional autophagy and its contribution to senescence, we focused on VSMCs in the aorta of mice. We previously demonstrated that senescent cells are observed in all layers of the aorta of *ppargc1a*^{-/-} mice, including VSMCs in the media and fibroblasts in the adventitia [6]. Histological examination of *Ppargc1a*^{+/+} (Figures 1A and B) and *Ppargc1a*[±] (Figures 1C and D) aorta samples revealed that the media of *Ppargc1a*[±] samples contain less organized VSMCs with more deposition of extracellular matrix (EM) compared with wild type (WT). The media of the aorta contains several layers of elastic laminae (EL; dark blue lines labeled with arrowheads in Figures 1A and 1C). VSMCs between two layers of elastic laminae were traced in Figures 1A and D to highlight the overall organization of VSMCs. Additionally, structures resembling apoptotic bodies were also seen in the *Ppargc1a*[±] aorta (Figure 1C, arrow). To better assess structural changes, we examined transverse sections of aortas by transmission electron microscopy (TEM) (Figure 1E–G). The most striking differences in overall organization were observed in smooth muscle cells in the media, which can be seen between two layers of EL. We observed less cell-cell contacts and disorganized mitochondria in *Ppargc1a*-deficient (Figure 1F and G) compared with WT (Figure 1E) mice. These changes were associated with increased EM deposition in *Ppargc1a*-deficient mice (30.8 ± 3.4%, n = 10) compared with WT (15.9 ± 7.7%, n = 4) (Figure 1H), which is consistent with the senescence-associated secretory phenotype (SASP) of senescent cells. Mitochondria were abundant in both genotypes, suggesting that *Ppargc1b* could be upregulated to induce mitochondrial biogenesis, as a compensatory mechanism. To test this possibility, we isolated mouse vascular smooth muscle cells (MASMs) from both genotypes and found that *Ppargc1b* mRNA was not upregulated (Fig. S1A and B), suggesting that degradation of mitochondria by autophagy could be inhibited. Consistent with previous reports, *ppargc1a*^{-/-} MASMs showed reduced expression of the antioxidant enzyme SOD2 (superoxide dismutase 2, mitochondrial) increased expression of the senescent marker CDKN1A/p21 (cyclin dependent kinase inhibitor 1A [P21]) (Fig. S1C), reduced cell proliferation (Fig. S1D) and increased expression of the DNA damage marker phosphorylated γ H2AFX/H2AX (H2A histone family, member X) in nuclear foci (Fig. S1E).

Autophagy is downregulated by *Ppargc1a* deficiency

To test whether autophagy is regulated by PPARGC1A, we used MASMs isolated from aortas of WT and *ppargc1a*^{-/-} mice and measured ROS levels, senescence, and autophagy markers in response to its overexpression using adenovirus containing *Ppargc1a* (Ad.PGC1A). Compared with WT, ROS levels were more than three-fold higher in *ppargc1a*^{-/-} cells (n = 13, p < 0.01) and were significantly downregulated by overexpression of PPARGC1A (Figure 2A). Similarly, the

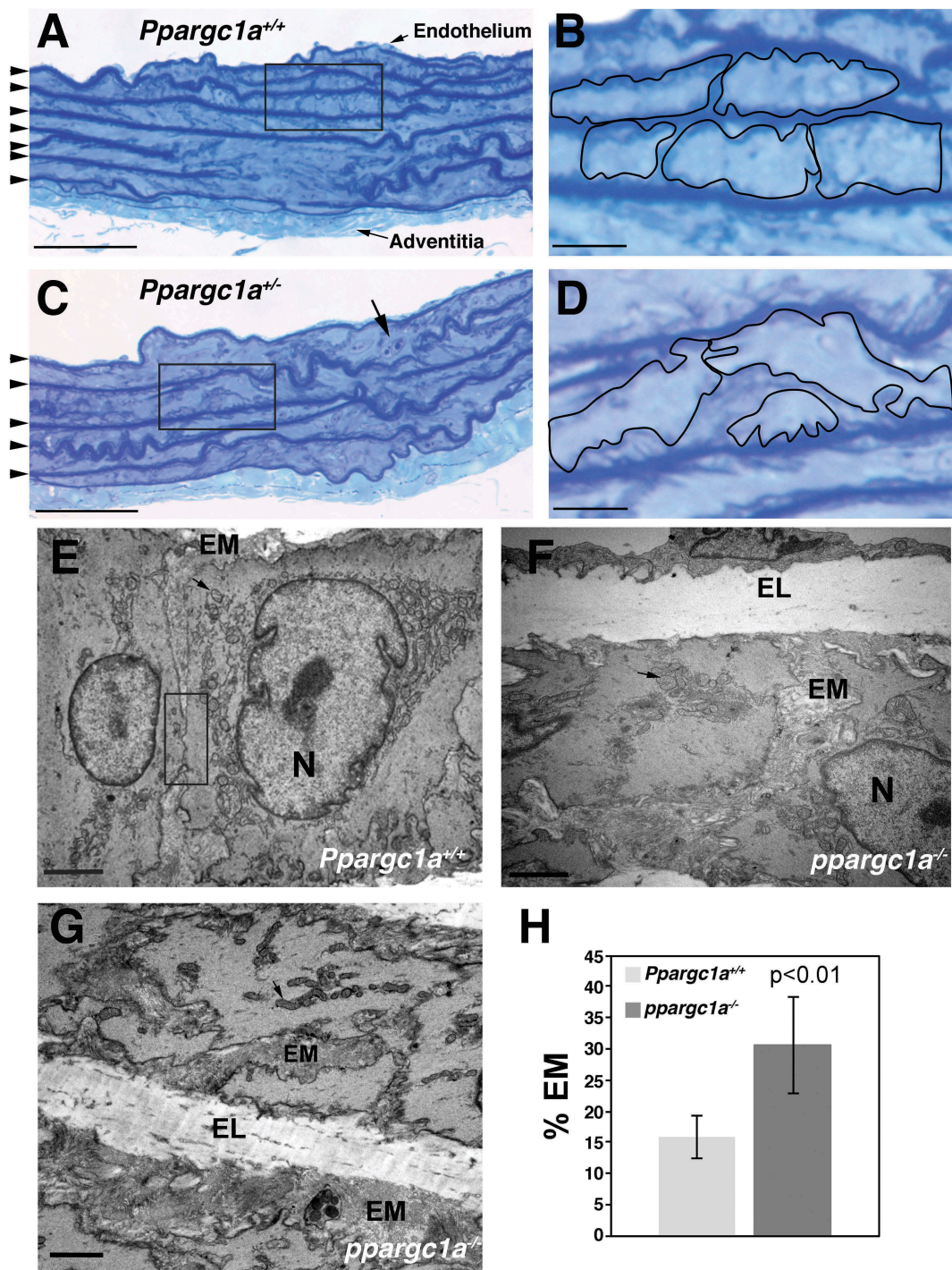


Figure 1. Structural differences in the media of *ppargc1a*^{-/-} mouse aorta. Aortas of 6-month-old *Ppargc1a*^{+/+} (A and B) and *Ppargc1a*^{+/-} (C and D) male mice were fixed, stained with 0.5% aqueous Toluidine Blue O and photographed at low (A and C) and high (B and D) magnification. Dark blue lines of elastic lamina are indicated with arrowheads in A and C. VSMCs in B and D were traced to indicate that more extracellular material is present in *Ppargc1a*^{+/-} samples. TEM images of VSMCs in the media of *Ppargc1a*^{+/+} (E) and *ppargc1a*^{-/-} (F and G) aortas were acquired using a Hitachi H-7500 electron microscope. Quantification of EM for both genotypes is shown in H. EM, extracellular matrix; N, nucleus; EL, elastic lamina. Bar: 50 μ m in A and C, 10 μ m in B and D, 2 μ m in E-G.

increase in activity of the senescence associated GLB1/ β -galactosidase (SA-GLB1) observed in *ppargc1a*^{-/-} cells was significantly reduced ($n = 13$, $p < 0.01$) by PPARGC1A overexpression (Figure 2B), which was also associated with upregulation of cell proliferation (Figure 2C) and SOD2 expression (Figures 2D and E), compared with control *ppargc1a*^{-/-} cells. Significant differences were also observed in SOD2 expression in WT cells in response to PPARGC1A

overexpression, but not for ROS levels (Figure 2A), SA-GLB1 (Figure 2B) or cell proliferation (Figure 2C).

To determine whether autophagy is impaired in *ppargc1a*^{-/-} VSMCs, we measured the conversion of LC3-I to II and expression of SQSTM1. Reduced LC3 conversion and accumulation of SQSTM1 are hallmarks of defective autophagy [20]. LC3-II:I ratio was strongly downregulated in *ppargc1a*^{-/-} cells, compared with WT ($n = 3$, $p < 0.01$), and the

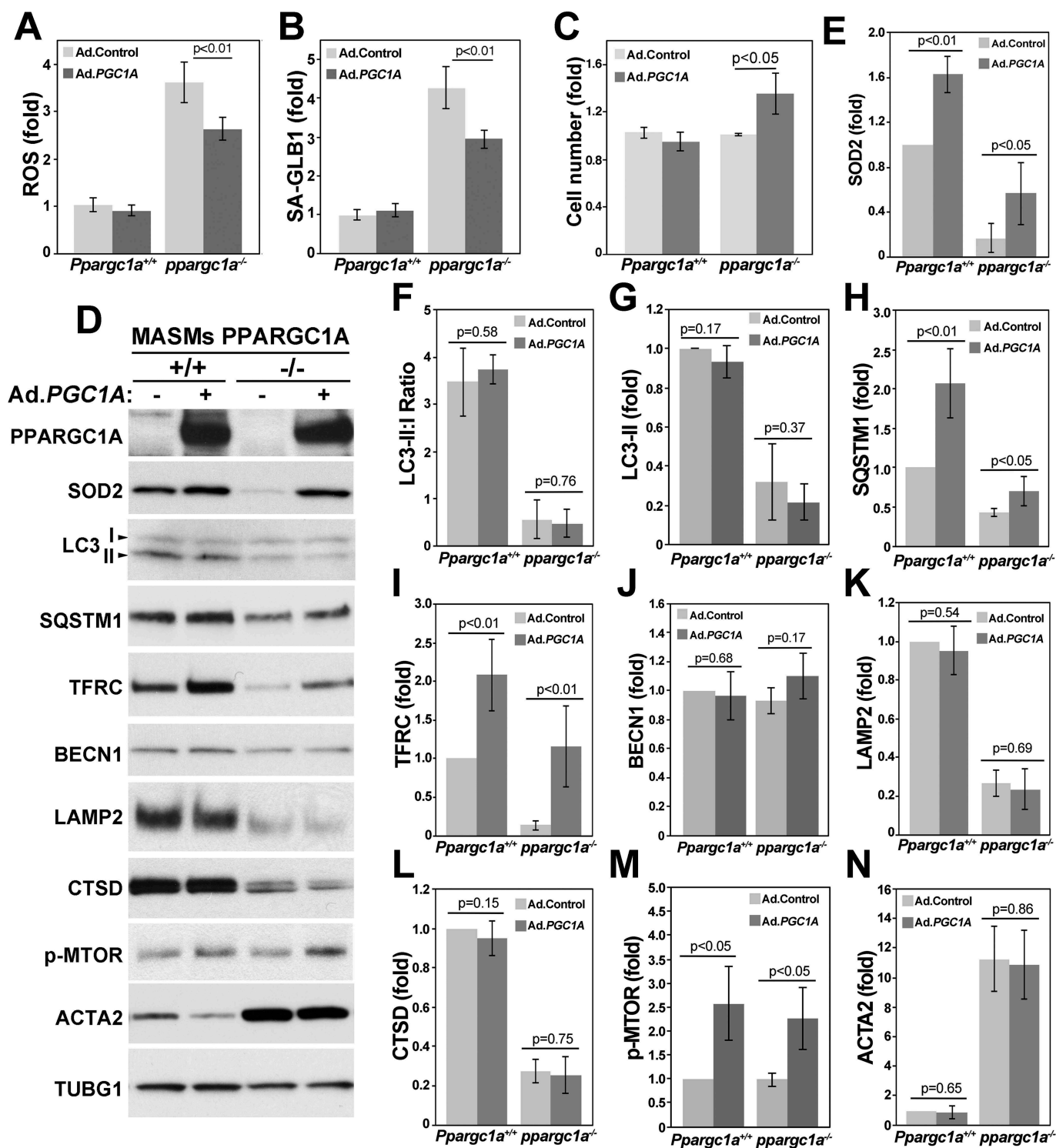


Figure 2. *Ppargc1a* deficiency increases senescence and reduces autophagy in VSMCs. *Ppargc1a*^{+/+} or *Ppargc1a*^{-/-} VSMCs were infected with 5×10^7 plaque-forming units (PFU)/ml of adenovirus control (Ad.Control) or adenovirus containing *PPARGC1A* (Ad.PGC1A). 3 d after infection, cells were processed for measurements of ROS levels using H₂DCFDA (A), SA-GLB1 activity using FDG (B), cell proliferation (C) or protein expression by western blot (D). ROS levels, SA-GLB1 and protein expression shown in D, adjusted by TUBG1 (F-N), were calculated as fold change, compared with WT cells infected with Ad.Control in 3 to 4 independent experiments performed in cells between passage 4 and 7.

ratio in both cell types was not altered by *PPARGC1A* overexpression (Figures 2D and F). Reduced LC3-II:I ratio was associated with reduced levels of LC3-II, which was not affected by *PPARGC1A* overexpression (Figure 2G). Surprisingly, reduced LC3-I to II conversion and LC3-II levels were not associated with *SQSTM1* accumulation. Instead

SQSTM1 behaved as a *PPARGC1A*-regulated gene (Figures 2D and H), similar to *SOD2* (Figures 2D and E) and *TFRC* [21,22] (Figures 2D and I). Expression of both *SQSTM1* and *TFRC* was reduced in *Ppargc1a*^{-/-} cells and was increased by *PPARGC1A* overexpression in WT and in *Ppargc1a*-deficient cells ($n = 4$, $p < 0.01$). Expression of the

autophagy-related gene BECN1/Beclin1 was not affected by *Ppargc1a* deficiency or its overexpression (Figure 2D and J). Similar to LC3, expression of the lysosomal protein LAMP2 and the precursor forms (52 kDa and 48 kDa) of the lysosomal protease CTSD (Figure 2D, K and L) was strongly reduced in *ppargc1a*^{-/-} cells (n = 4, p < 0.01, respectively). Expression of these markers was not upregulated by PPARGC1A overexpression, suggesting that lysosomal dysfunction could be a consequence of senescence and not directly regulated by PPARGC1A. It is also possible that expression of PPARGC1A above physiologic levels may activate a signaling pathway preventing the upregulation of lysosomal proteins and LC3 conversion. In fact, we observed a significant increase in phosphorylated/active MTOR in response to PPARGC1A overexpression in WT and *Ppargc1a*-deficient cells (n = 3, p < 0.05) (Figures 2D and M). Activation of MTOR, an autophagy inhibitor, may explain in part why LC3 conversion is not upregulated in PPARGC1A-overexpressing cells.

In addition to changes in the expression of autophagy and lysosomal genes, the level of ACTA2/SM-actin (actin, alpha 2, smooth muscle, aorta), mainly found at the cell periphery and in the cortical actin cytoskeleton, was strongly upregulated (n = 3, p < 0.01) by *Ppargc1a* deficiency, and was not significantly reduced by PPARGC1A overexpression (Figure 2D and N). Upregulation of ACTA2 is also observed during senescence in other cell types, including fibroblasts [23], suggesting that ACTA2 can be used as an additional marker of cellular senescence in VSMCs.

Altogether these data suggest that PPARGC1A-induced senescence is associated with impaired autophagy and lysosomal dysfunction. The fact that increased ROS levels and senescence induced by *Ppargc1a* deficiency were partially rescued by PPARGC1A overexpression suggests that upregulation of SQSTM1 and/or antioxidant genes like SOD2 may contribute to these effects.

To assess whether defective autophagy can be observed *in vivo*, we processed aortas of WT and *ppargc1a*^{-/-} mice by TEM. This analysis revealed that autophagosome structures, characterized by a double membrane organelle containing cargo, were observed in WT VSMCs (Figure 3A, arrow shows an autophagosome containing a mitochondrion) although in low number (0.3 ± 0.1, n = 20 fields). *ppargc1a*^{-/-} samples, on the other hand, showed abnormal autophagosome-like structures surrounded by a double membrane and containing electron-dense material and concentric membrane layers (Figure 3B). Interestingly, autophagosome-like structures were also observed in the EM (Figure 3C). On average, *ppargc1a*^{-/-} aortas showed a tendency toward higher number of autophagosome-like structures/field (1.05 ± 0.44, n = 17 fields) with no significant differences, compared to WT (p = 0.085) (Figure 3D). These data suggest that the formation or maturation of autophagosomes and/or degradation of autophagic content could be altered by *Ppargc1a* deficiency. Overall, TEM analysis demonstrated the presence of defective autophagosome-like structures *in vivo* in aortas of *ppargc1a*^{-/-} animals.

Next, we measured the number of autophagosomes in WT and *ppargc1a*^{-/-} VSMCs *in vitro* by immunofluorescence. Consistent with the notion that PPARGC1A regulates

autophagy, LC3- and SQSTM1-positive compartments (puncta) were significantly diminished in the absence of PPARGC1A (Figure 3E and F). The contradictory observation in the number of autophagosome structures *in vivo* and *in vitro* may be a consequence of differences in autophagic flux of cells in the aorta, which are in a quiescent state, compared with VSMCs in culture, which are in a proliferating state.

To test whether reduced SQSTM1 expression and SQSTM1-positive puncta *in vitro* correlated with reduced SQSTM1 expression *in vivo*, we measured its protein levels in aortas. Similar to VSMCs in culture, SQSTM1 level was significantly reduced in aortas of *ppargc1a*^{-/-}, compared with WT mice (n = 3 per genotype, p < 0.05) (Figures 3G and H). In contrast, LC3-I to II conversion, as well as LC3-II levels were not affected (Figures 3G, I and J). To test whether SQSTM1 is regulated at the transcriptional level by PPARGC1A, we measured mRNA levels in VSMCs from both genotypes and found a significant reduction of approximately 50% in knockout cells (Figures 3K and L).

Altogether these data showed that *Ppargc1a* deficiency reduced SQSTM1 protein and mRNA levels and the number of autophagosomes and LC3-II levels in VSMCs *in vitro* and promoted the formation of dysfunctional autophagosome-like structures in VSMCs in aortas *in vivo*.

SQSTM1 is reduced by age and by *Ppargc1a* deficiency in mouse brain

To determine whether PPARGC1A regulates SQSTM1 expression and autophagy in other tissues, we isolated brain samples from young (6 months) and old (18 months) WT and *ppargc1a*^{-/-} mice (Figure 4). The expression of SQSTM1 and LC3-I was significantly downregulated by age and by *Ppargc1a* depletion (n = 4, p < 0.01), which was not further reduced by age in knockout mice (Figure 4A-C). A longer exposure of the LC3 western blot revealed that LC3-II is expressed at lower levels in these samples. This observation is in line with data from other investigators showing that LC3-I expression is more prominent than LC3-II in brain homogenates [24–26]. Although TFRC expression was reduced by age, which did not reach significance (p = 0.13), it was strongly downregulated in young and old (n = 4, p < 0.01) *ppargc1a*^{-/-} mice (Figures 4A and D). Similar effects, compared with SQSTM1 and LC3-I, were observed for SOD2 expression (Figure 4A and E).

Expression of *Sqstm1* mRNA is reduced during aging (17 months, compared with 3 months) in liver samples of C57Bl/6 mice [17]. Thus, we tested whether reduced protein levels of SQSTM1, LC3 and PPARGC1A correlated with reduced mRNA content. Consistent with the report by Kwon *et al.* [17], a reduction of about 40%, 50% and 30%, respectively, was seen for these three markers (Figure 4F and G).

***Ppargc1a* deficiency impairs lysosomal function and autophagic flux**

As mentioned before, CTSD is a lysosomal protease that is synthesized as a 52-kDa precursor that is cleaved into a mature 48-kDa form in the lysosome. This form is further

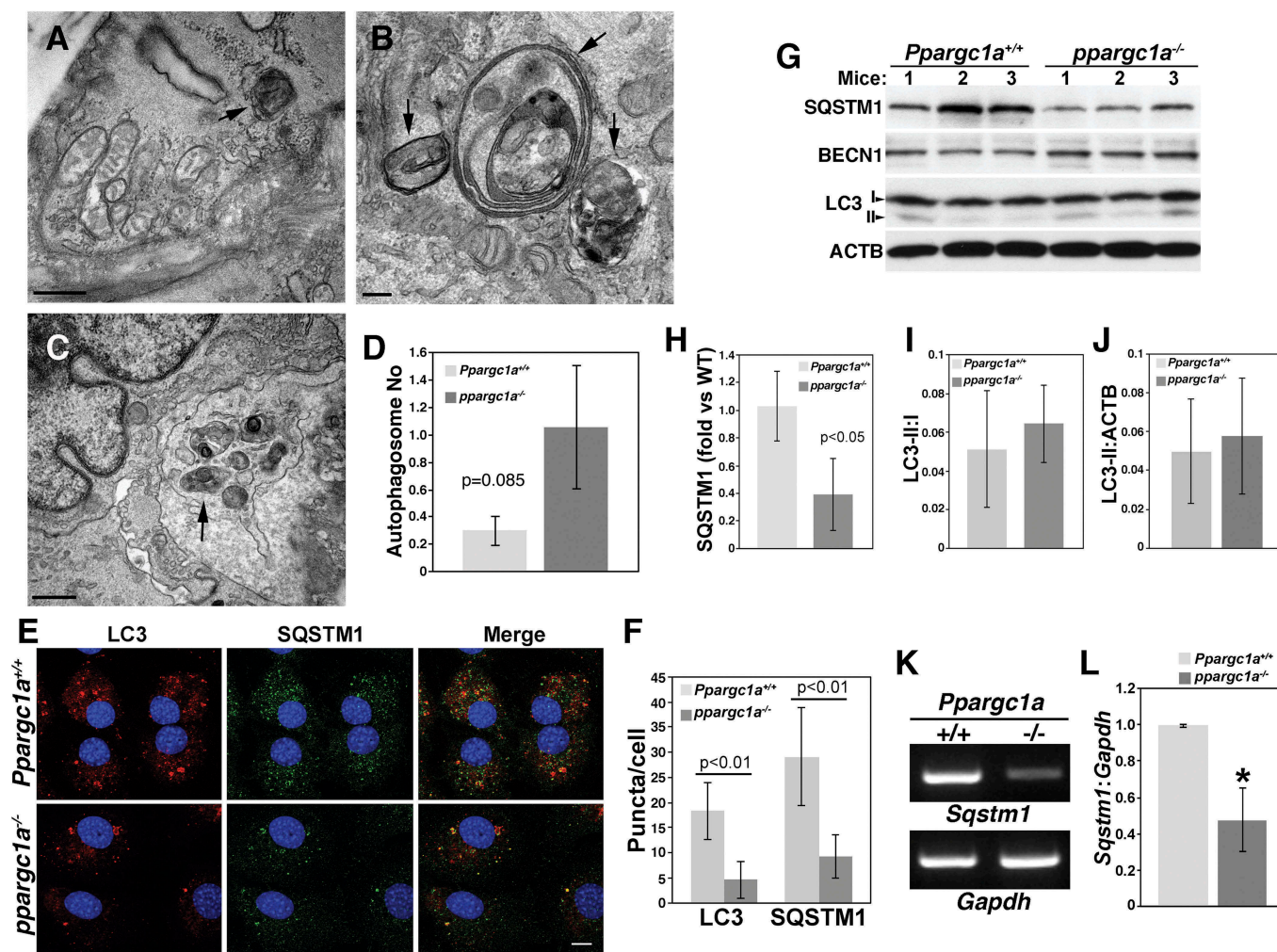


Figure 3. Abnormal autophagosomes and reduced SQSTM1 expression in the aorta of *ppargc1a^{-/-}* mice. Aortas of *Ppargc1a^{+/+}* (A) and *ppargc1a^{-/-}* mice (B and C) were analyzed by TEM. Arrows indicate autophagosomes. Bar: 0.5 μ m in A and C, and 0.2 μ m in B. Graph presenting the overall average of autophagosomes in both genotypes is shown in D. *Ppargc1a^{+/+}* and *ppargc1a^{-/-}* VSMCs were fixed and incubated with mouse LC3 and rabbit SQSTM1 antibodies (E). Images in E were acquired using a confocal microscope for the quantification of LC3 and SQSTM1 puncta. Bar: 10 μ m. (F). 34 cells and 30 cells were analyzed for LC3 in WT and knockout, respectively, while 23 and 24 cells were analyzed for SQSTM1 puncta in WT and knockout, respectively. Aortas of 6-month-old *Ppargc1a^{+/+}* and *ppargc1a^{-/-}* male mice were lysed and processed for western blot analysis (G). SQSTM1, LC3-I and LC3-II levels were adjusted by ACTB and expressed as fold change, compared with WT (H-J). mRNA was isolated from *Ppargc1a^{+/+}* and *ppargc1a^{-/-}* VSMCs and used to measure *Sqstm1* and *Gapdh* mRNA levels (K and L). 3 independent mRNA preparations per genotype. * denotes p < 0.01 in L.

processed to produce the active enzyme formed by a heavy chain of 34 kDa and a light chain of 14 kDa. To further assess lysosomal function, we measured the expression of these two mature forms, as well as lysosomal morphology. Similar to the precursor forms, the 34-kDa form was also significantly reduced, while the 14-kDa form was undetected in *ppargc1a^{-/-}* VSMCs (Figure 5A and B). As expected, reduced lysosomal function led to the accumulation of the autophagy receptor NBR1 (Figures 5A and C). Expression of these markers was not affected by PPARGC1A overexpression.

In terms of lysosomal function, reduced expression of CTSD and LAMP2 was associated with enlarged lysosomes (Figure 5D), a characteristic of lysosomal dysfunction [27]. Swollen lysosomes can be observed at the perinuclear area in *ppargc1a^{-/-}* VSMCs (see Figure 5D inserts). Next, we determined whether changes in the expression of autophagy and

lysosomal genes were also regulated at the mRNA level. In contrast to SQSTM1, mRNA expression of *Lc3*, *Becn1*, *Nbr1*, the autophagy receptor *Optn* (optineurin), *Lamp2* and *Ctsd* was not affected by *Ppargc1a* deficiency (Figure 5E and F).

Next, we measured autophagic flux by treating cells with 50 μ M chloroquine (Chl), an inhibitor of lysosomal degradation, for 2 to 8 h. As expected, the rate of accumulation of LC3-II and SQSTM1 over time was significantly higher in WT compared with *ppargc1a^{-/-}* cells (Figure 5G-I), suggesting that decreased LC3 expression and not increased lysosomal degradation mediates SQSTM1 downregulation. Although NBR1 protein levels were elevated in knockout cells at baseline, the rate of NBR1 accumulation was similar between genotypes (Figure 5G and J). Interestingly, inhibition of lysosomal degradation reduced CTSD expression at a similar rate in both cell types, suggesting that reduced expression of the lysosomal proteins LAMP2 and CTSD

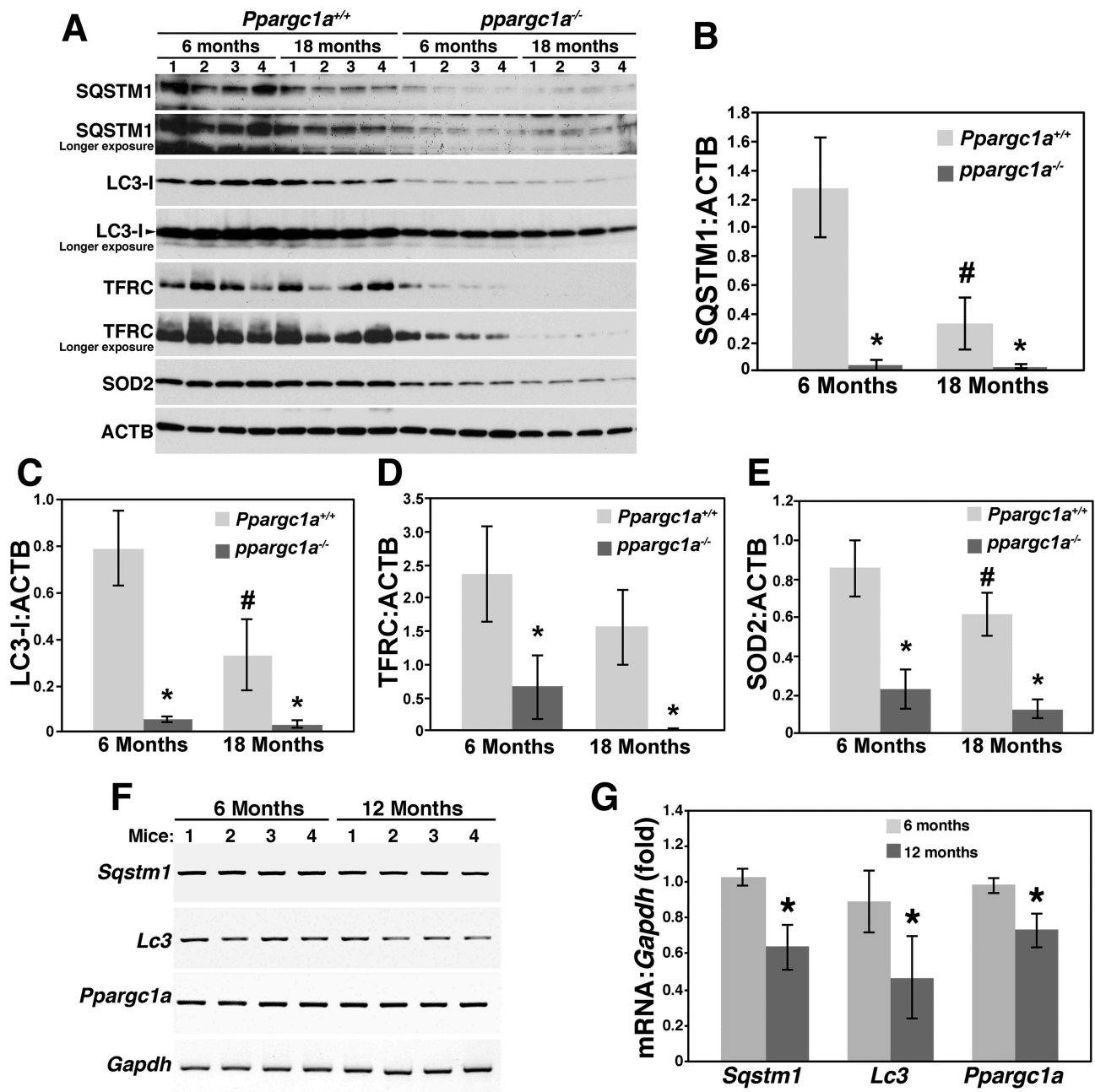


Figure 4. Reduced LC3 and SQSTM1 expression in the brain of *Ppargc1a*^{-/-} deficient mice. Brain samples from 6- and 18-month-old *Ppargc1a*^{+/+} and *Ppargc1a*^{-/-} male mice were homogenized and total extracts separated in 4–20% precast Criterion gels for the analysis of SQSTM1, LC3, TFRC and SOD2 expression (A). Protein expression of each gene was adjusted by ACTB (B–E). * and ‡ denote significant differences between WT and *Ppargc1a*^{-/-}, and between 6- and 18-month-old WT, respectively. mRNA from brain samples of 6- and 12-month-old male C57Bl/6 mice were tested for the expression of *Sqstm1*, *Lc3* and *Ppargc1a* (F). mRNA levels were adjusted by *Gapdh* and expressed as fold change compared with animals of 6 months of age (G). * denote $p < 0.05$.

could be a consequence of lysosomal dysfunction and not directly regulated by PPARGC1A.

Reduced autophagy induces senescence

To determine whether defective autophagy contributes to senescence development in VSMCs, we tested whether inhibition of autophagy can induce senescence and whether rapamycin can reduce the effects of AGT II, a well-known inducer of oxidative stress and senescence in VSMCs [28]. To inhibit autophagy, we

used 3-MA and spautin-1 (specific and potent autophagy inhibitor-1), which inhibit autophagy through different molecular mechanisms. 3-MA inhibits class III Ptdln3K (phosphatidylinositol 3-kinase) [29] reducing the formation of Ptdln3P on the phagophore membrane, a process needed for the elongation of this membrane and the initiation of autophagy. Spautin-1 inhibits USP10 and USP13, two ubiquitin peptidases that deubiquitinate BECN1 in the class III Ptdln3K-PIK3C3/VPS34 complex leading to degradation of BECN1 and inhibition of the PIK3C3 complex in HeLa cells and mouse embryonic fibroblasts [30]. We used

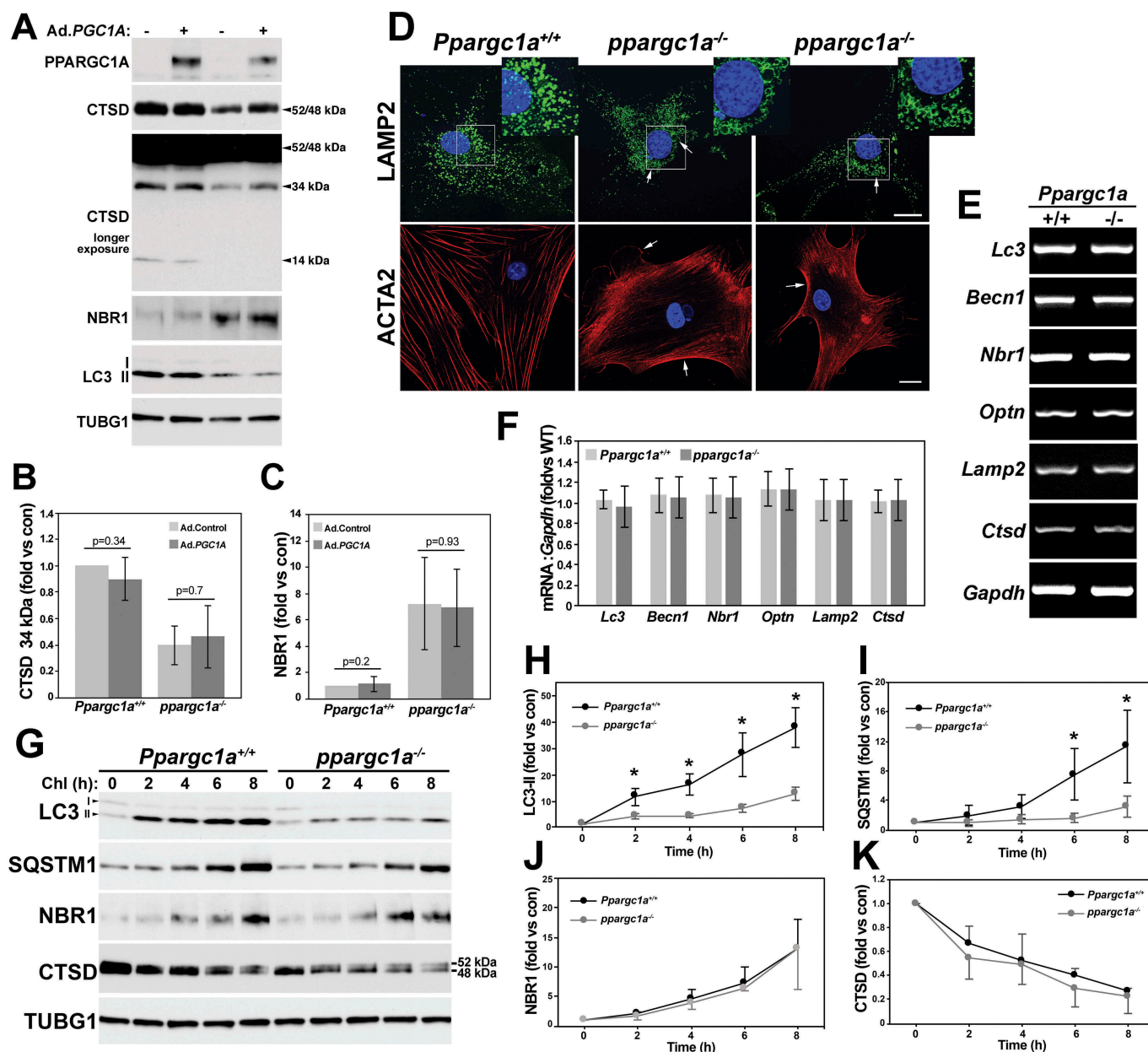


Figure 5. PPARGC1A regulates autophagic flux. *Ppargc1a*^{+/+} and *Ppargc1a*^{-/-} VSMCs were infected with 5×10^7 PFU of Ad.Control or Ad.PGC1A. 3 d after infection cells were lysed and samples tested for the indicated antibodies (A). The expression of the 34-kDa form of CTSD and NBR1 was adjusted by TUBG1 and expressed as fold change, compared with WT cells infected with Ad.Control (B and C). *Ppargc1a*^{+/+} and *Ppargc1a*^{-/-} VSMCs were fixed in 4% PFA and incubated with antibodies against LAMP2 or ACTA2, and images were acquired using a confocal microscope. Bar: 10 μ m (D). mRNA from both genotypes was tested for the expression of the autophagy and lysosomal markers shown in E ($n = 3$ samples per genotype). mRNA levels were adjusted by *Gapdh* and expression expressed as fold change, compared with WT cells (F). Cells were treated with 50 μ M Chl in DMEM containing 0.5% FBS for 2 to 8 h. Cells were then lysed and separated in 4–20% Precast Criterion gels (G). LC3-II, SQSTM1, NBR1, and CTSD protein levels were adjusted by TUBG1 (H–K). Expression of each marker in untreated cells was assigned as 1. Fold changes were then calculated for each genotype to assess the rate of protein accumulation or reduction. * denotes $p < 0.05$.

rapamycin, an MTOR inhibitor, to stimulate autophagy. MTOR inhibits autophagy by targeting the ULK1 complex [31], which is needed for the formation of the autophagosome.

We have used rat aortic smooth muscle cells (RASMs) to study the mechanism by which AGT II and zinc overload induce senescence [28,32]. We showed that AGT II induces the acetylation/inactivation of PPARGC1A leading to reduced CAT (catalase) [33] and SIRT1 (Sirtuin 1) expression and increased senescence. Thus, we first tested whether PPARGC1A also regulates SQSTM1 expression in RASM cells (Fig. S2). Similar to MASMs, PPARGC1A increased the

expression of known targets including CAT, SOD2, TFRC and CYCS (cytochrome c, somatic), while downregulating CDKN1A expression, as we previously reported [6] (Fig. S2A). PPARGC1A also upregulated the expression of SQSTM1 and phosphorylated MTOR, but not LC3-II (Figs. S2A–D). It is likely that increased MTOR activity prevented the upregulation of LC3-II. Further, similar to MASMs *Lc3* mRNA was unaffected by PPARGC1A (Figs. S2E and F). As we previously reported [28,34], AGT II increased SA-GLB1 activity compared with control cells, which was significantly downregulated by rapamycin in RASMs (Figures 6A and B).

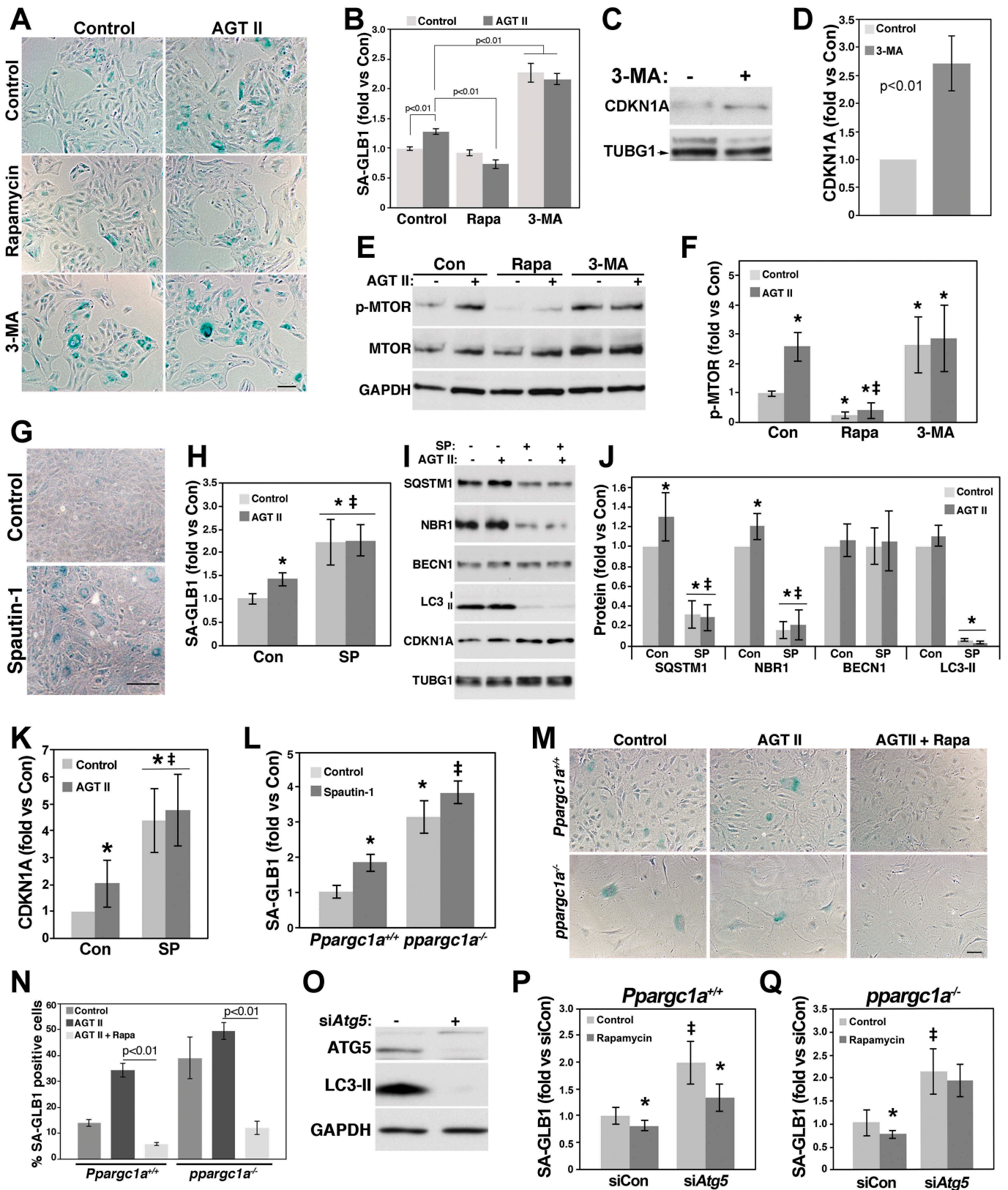


Figure 6. Impaired autophagy induces senescence of VSMCs. RASMs treated with and without 10 mM 3-MA or 100 nM rapamycin (Rapa) were treated with and without 100 nM AGT II for 3 d. Cells were then fixed and tested for SA-GLB1 activity measurements (A and B) or were lysed for the analysis of CDKN1A expression (C and D) and MTOR phosphorylation (E and F) by western blot. RASMs were incubated with 10 μ M spautin-1 (SP) for 3 d for measurements of SA-GLB1 activity (G and H) or were treated with and without 100 nM AGT II and 10 μ M spautin-1 for 3 d for protein expression analysis (I). Protein levels shown in I were adjusted by TUBG1 and expressed as fold change compared with control untreated cells (J and K). * and ‡ denote significant differences compared with control and AGT II, respectively. *Ppargc1a*^{+/+} and *ppargc1a*^{-/-} VSMCs were treated with 10 μ M spautin-1 (L) or with and without 100 nM AGT II and 100 nM rapamycin (M and N) for 3 d for SA-GLB1 activity measurements. WT VSMCs were transfected with 200 nM siControl or siAtg5 and protein expression of ATG5 was determined by western blot (O). *Ppargc1a*^{+/+} and *ppargc1a*^{-/-} VSMCs transfected with siControl or siAtg5 were treated with 100 nM rapamycin for 3 d (P and Q). SA-GLB1 was then expressed a fold change compared with untreated siControl cells. * and ‡ denote significant differences between cells treated with and without rapamycin and between siControl and siAtg5-transfected cells, respectively. Bar: 20 μ m in A and 100 μ m in G and M.

3-MA increased SA-GLB1 activity (Figures 6A and B) and CDKN1A expression (Figures 6C and D) in basal conditions, effects that were not further increased by AGT II (Figures 6A and B). Both AGT II- and 3-MA-induced senescence was associated with elevated MTOR phosphorylation (Figures 6E and F). Similarly, spautin-1 upregulated SA-GLB1 activity basally and showed no additive effects in AGT II-induced senescence (Figures 6G and H). Next, we tested whether spautin-1 could also induce the degradation of BECN1 in RASMs. Surprisingly, a robust downregulation in the expression of SQSTM1, NBR1 and LC3-II, but not BECN1, was observed in spautin-1-treated cells (Figure 6I and J). AGT II showed a modest, but significant increase in SQSTM1 and NBR1 expression in control cells, but not in cells treated with spautin-1 (Figure 6I and J). Similar to SA-GLB1, CDKN1A expression was significantly upregulated by AGT II and spautin-1 and no additive effects were seen in AGT II- and spautin-1-treated cells (Figure 6I and K). Spautin-1 also upregulated SA-GLB1 activity in WT MASMs and showed a modest but significant effect in *ppargc1a*^{-/-} cells (Figure 6L), suggesting that impaired autophagy is a major driver of senescence in the absence of *Ppargc1a*.

Next, we tested whether rapamycin could also reduce senescence induced by AGT II and *Ppargc1a* deficiency in MASMs (Figure 6M and N). Similar to RASMs, AGT II increased SA-GLB1 activity in WT MASMs, which was significantly downregulated by rapamycin. In contrast, SA-GLB1 activity was elevated basally in *ppargc1a*^{-/-} cells but was not significantly upregulated by AGT II. Rapamycin reduced AGT II-induced senescence, as well as basal senescence ($7.7 \pm 3.4\%$, $n = 3$, $p < 0.01$). As expected, MTOR phosphorylation was reduced by rapamycin in both WT and *ppargc1a*^{-/-} cells (Fig. S3A). Further, LC3-II and SQSTM1 levels were upregulated by rapamycin and reduced by 3-MA (Figs. S3B-D). The unexpected effects of these drugs in SQSTM1 protein levels suggest that SQSTM1 is not a good indicator of autophagic flux in VSMCs.

Since MTOR can regulate other processes, in addition to autophagy, that could also be involved in senescence, we tested the effect of rapamycin in cells depleted of ATG5, a core component of the autophagy machinery. Similar to spautin-1, *Atg5* siRNA showed a robust downregulation in LC3-II levels (Figure 6O), and upregulation in SA-GLB1 activity (Figure 6P), an effect that was significantly reduced by rapamycin. Interestingly, rapamycin was unable to reduce senescence in *ppargc1a*^{-/-} cells depleted of ATG5 (Figure 6Q).

Altogether these data showed that autophagy impairment promotes senescence of VSMCs and that upregulation of autophagy by rapamycin reduces senescence induced by AGT II and by *Ppargc1a* deficiency. Further, these data also suggest that MTOR regulates senescence by autophagy-dependent and independent mechanisms.

Sqstm1 deficiency induces senescence

Ppargc1a deficiency is associated with dysfunctional autophagy and increased senescence that can be rescued by rapamycin, as well as with reduced SQSTM1 expression. To

determine the contribution of SQSTM1 to *Ppargc1a* deficiency effects, we downregulated *Sqstm1* by siRNA in RASM cells and determined senescence in response to AGT II and zinc overload, another inducer of senescence in VSMCs [28,32]. Si*Sqstm1* reduced SQSTM1 protein expression by 80% compared with siControl-treated cells ($n = 4$, $p < 0.01$) (Figure 7A and B), while increasing CDKN1A levels more than 2-fold (Figures 7A and C). Basal SA-GLB1 activity was upregulated by *Sqstm1* siRNA compared with siControl-treated cells ($n = 12$, $p < 0.01$) (Figure 7D). Senescence induced by AGT II and zinc was also elevated in si*Sqstm1*-treated cells (Figure 7D). These additive effects suggest that SQSTM1 acts through a different mechanism compared with AGT II and zinc to regulate senescence of VSMCs. Next, we determined whether senescence induced by *Ppargc1a* deficiency could be rescued by SQSTM1. Overexpression of SQSTM1 using adenovirus (Ad.SQSTM1) promoted a small but significant reduction in ROS levels (Figure 7E) and SA-GLB1 activity (Figure 7F). Ad.SQSTM1 increased SQSTM1 expression more than 8-fold and LC3-II levels more than 2-fold, compared with cells treated with Ad.Control (Figure 7G-I). In contrast, *ppargc1a*^{-/-} cells infected with Ad.SQSTM1 in the same conditions as WT cells showed a less robust, but significant upregulation of SQSTM1 expression (Figure 7G and H) and LC3-II levels (Figures 7G and I), compared with control cells. These data suggest that overexpressed SQSTM1 is degraded in *ppargc1a*^{-/-} cells by an unknown mechanism. This effect can explain the small reduction in ROS levels and senescence observed in *ppargc1a*^{-/-} cells overexpressing SQSTM1 (Figure 7E and F).

To determine the physiological significance of SQSTM1 *in vivo*, we measured senescence in aortas of 2-month-old *sqstm1*^{-/-} male mice. SA-GLB1 activity was upregulated ($n = 8$, $p < 0.01$) in *sqstm1*^{-/-}, compared with WT C57Bl/6 and *Sqstm1* heterozygote mice (Figure 7J). The senescence phenotype of *sqstm1*^{-/-} mice was not associated with the obesity phenotype of this animal model (Figure 7K) since body weight of WT (20.5 ± 2.6 g, $n = 8$), heterozygote (19.32 ± 1.9 g, $n = 8$) and *sqstm1*^{-/-} (21.7 ± 1.4 g, $n = 8$) mice was not significantly different at this age. *sqstm1*^{-/-} mice display mature-onset obesity with increased body weight at about 5 months of age, compared with WT C57Bl/6 mice [18]. Consistent with elevated SA-GLB1 activity, TRP53/p53 (transformation related protein 53) protein expression was also upregulated in aortas of *sqstm1*^{-/-} ($n = 4$, $p < 0.05$), but not heterozygote ($n = 4$, $p = 0.56$), compared with WT mice (Figures 7L and M). These changes were associated with a significant reduction in LC3-I expression in *sqstm1*^{-/-}, but not *Sqstm1*[±], compared with WT mice (Figures 7L and N). Similar to brain homogenates, LC3-II was barely detected in aorta samples. Quantification of LC3-II was not possible since no bands were detected in some of the samples.

To determine whether *Sqstm1*- and *Ppargc1a*-deficient VSMCs share the same or similar phenotypes, we isolated VSMCs from aortas of WT and *sqstm1*^{-/-} mice. Similar to *Ppargc1a* deficiency, *Sqstm1* depletion resulted in reduced

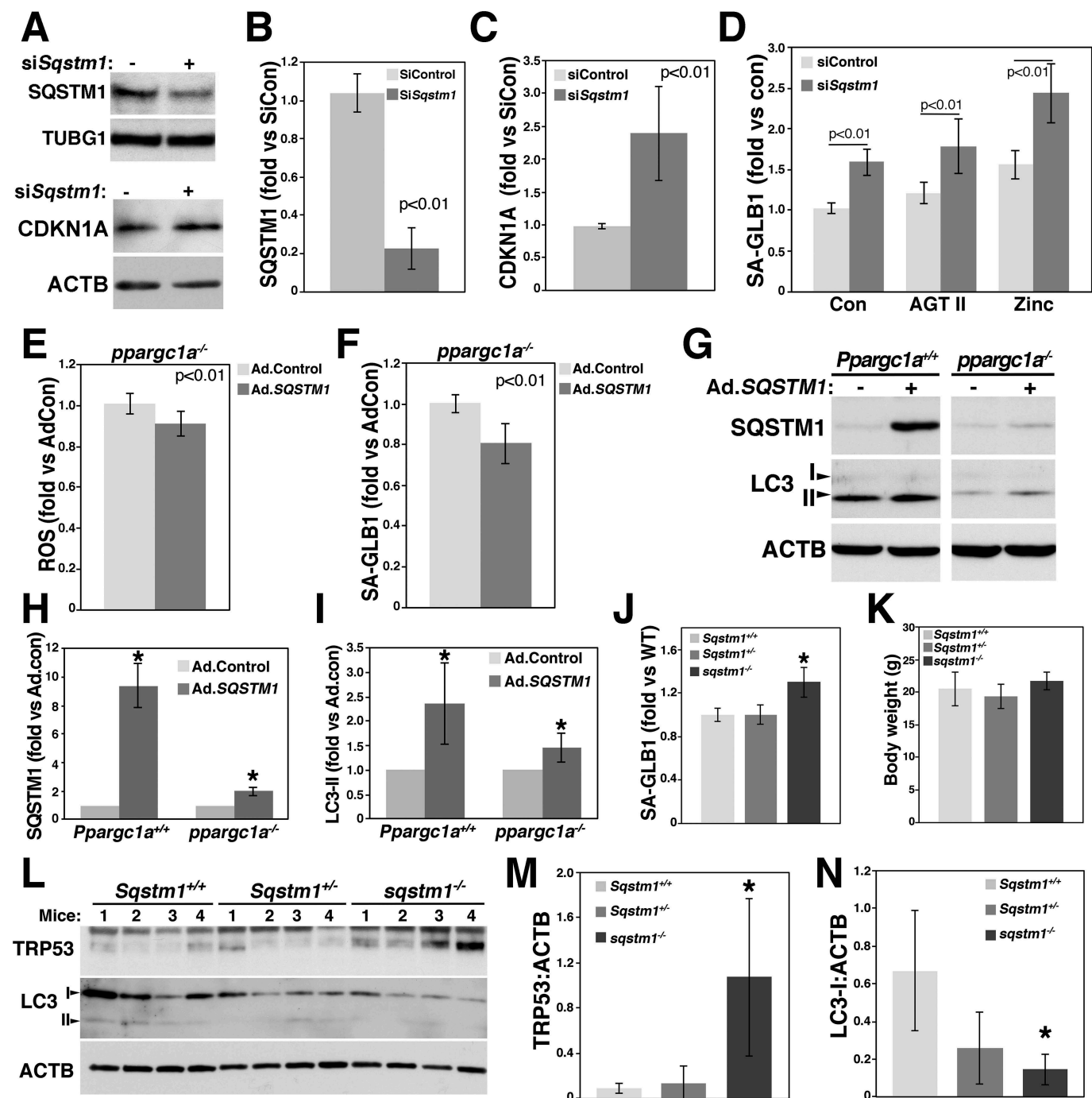


Figure 7. Reduced SQSTM1 expression increases ROS levels and senescence of VSMCs. RASMs were transfected with siRNA control or *siSqstm1* for measurements of SQSTM1 and CDKN1A expression (A-C), and SA-GLB1 activity, using FDG, in response to 100 nM AGT II or 50 μ M zinc for 3 d (D). *ppargc1a*^{-/-} VSMCs were infected with 1×10^7 PFU of adenovirus control (Ad.Control) or adenovirus containing human SQSTM1 gene (Ad.SQSTM1) for ROS measurements (E) and SA-GLB1 activity using FDG (F). *Ppargc1a*^{+/+} and *ppargc1a*^{-/-} VSMCs infected with Ad.Control or Ad.SQSTM1 were lysed for analysis of SQSTM1 and LC3-II expression. (G-I). Expression was expressed as fold change compared with siControl-transfected cells. Aortas of 2-month-old mice *Sqstm1*^{+/+}, *Sqstm1*^{+/-} and *sqstm1*^{-/-} in the C57Bl/6 background (8 males each) were cleaned, fixed and tested for SA-GLB1 activity using FDG (J). Fluorescence was adjusted by the weight of aortas. * denotes $p < 0.01$. Body weight for each genotype is expressed in grams (g) (K). Aortas of each genotype (2-month-old, males) were cleaned of periadventitial fat, lysed and 80 μ g of total extracts were separated in a 4–20% precast Criterion gels (L). Quantification of TRP53 and LC3-II adjusted by ACTB is shown in M and N, respectively. * denotes $p < 0.05$.

cell proliferation (Figure 8A), increased SA-GLB1 activity (Figures 8B and C) and ROS levels (Figures 8D and E), and defective autophagy (Figure 8F–J). *sqstm1*^{-/-} cells showed NBR1 accumulation, and reduced LC3-II levels and

no changes in BECN1 expression (Figures 8F and G). Different from *Ppargc1a* deficiency, cells lacking *Sqstm1* expressed more MTOR and its phosphorylated form (Figures 8F and G). Autophagic flux was also impaired in

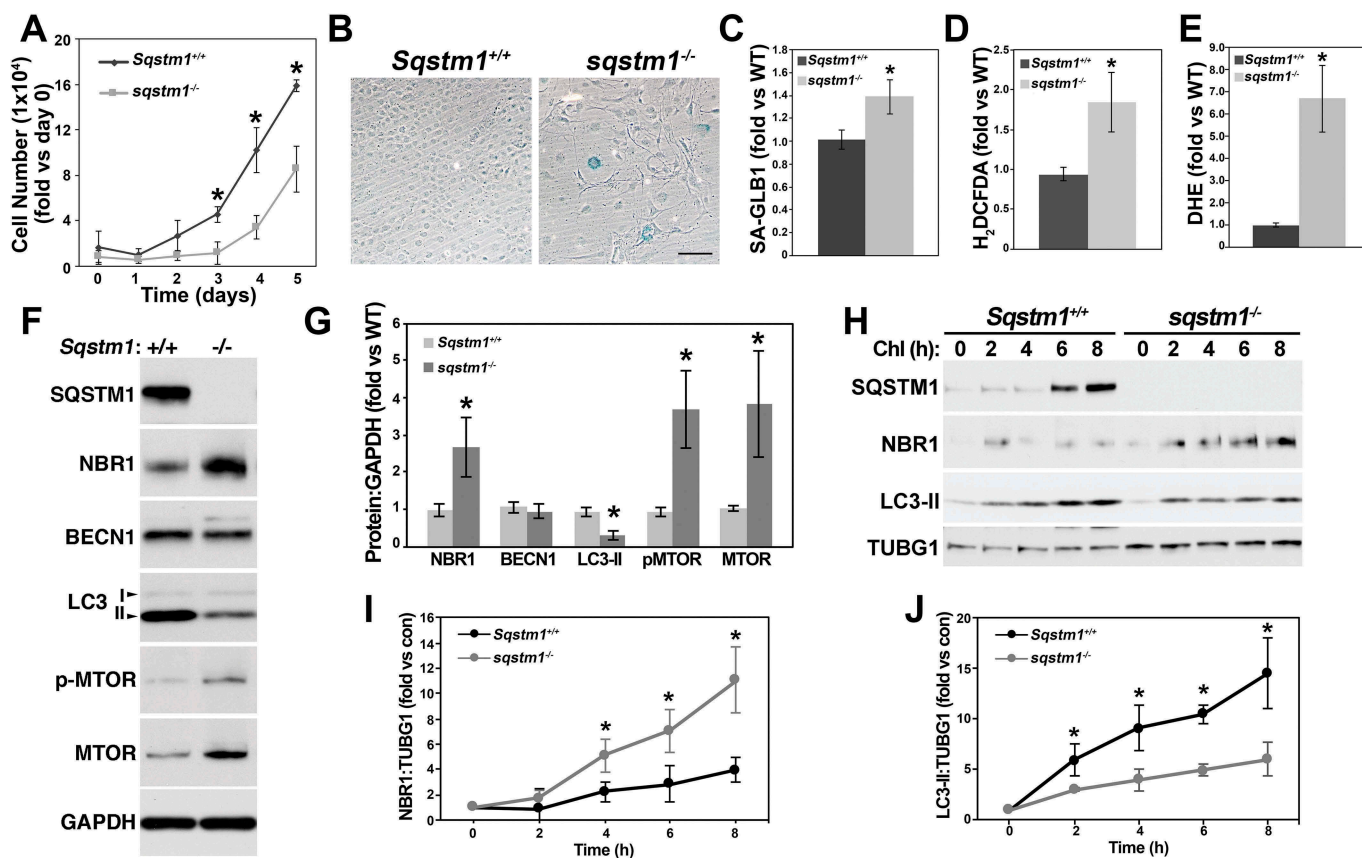


Figure 8. *Sqstm1* deficiency increases ROS levels and senescence and reduces autophagic flux. WT and *sqstm1^{-/-}* VSMCs were cultured in DMEM with 10% FBS for cell proliferation experiments (A) (triplicates in 3 independent experiments), analysis of SA-GLB1 activity (B and C), and hydrogen peroxide (D) and superoxide (E) levels, or for analysis of protein expression (F). Expression of markers in F was adjusted by GAPDH and expressed as fold change, compared with WT cells (G). WT and *sqstm1^{-/-}* VSMCs were treated with 50 μ M Chl for 2 to 8 h for the analysis of autophagic flux (H). The expression of NBR1 (I) and LC3-II (J) levels was adjusted by TUBG1. The value of untreated cells was calculated as 1. Fold change compared with untreated cells was then calculated for each genotype. * denoted $p < 0.05$. Bar: 100 μ m in B.

these cells, as measured by the increased and reduced accumulation of NBR1 and LC3-II, respectively, in response to Chl treatment (Figure 8H-J).

Altogether these data demonstrate that downregulation of SQSTM1 mediates *Ppargc1a* deficiency-induced senescence and that PPARGC1A and SQSTM1 have opposite effects in MTOR function.

Discussion

PPARGC1A is a well-known regulator of mitochondrial biogenesis and antioxidant capacity among other functions. However, little is known about the role of PPARGC1A in autophagy in the cardiovascular system. Here, we report that *Ppargc1a* deficiency causes defective autophagy, which was associated with reduced LC3-I to II conversion, LC3-II levels, SQSTM1 expression (protein and mRNA levels), autophagosome number, autophagic flux, and with accumulation of NBR1 in VSMCs in culture. Reduced SQSTM1 expression and the presence of abnormal autophagosome-like structures were also observed in VSMCs in aortas of *ppargc1a^{-/-}* mice *in vivo*. As we previously reported [6], *Ppargc1a* deficiency reduced cell proliferation and increased ROS levels and

senescence. Our data suggest that impaired autophagy promoted the senescence phenotype of *Ppargc1a* depleted cells since inhibition of autophagy by 3-MA, spautin-1 or *Atg5* siRNA caused senescence. The upregulation in SA-GLB1 seen in *ppargc1a^{-/-}* cells was further increased by spautin-1 and *Atg5* depletion. This effect is consistent with the observation that autophagic flux is reduced, but not completely inhibited, in *ppargc1a^{-/-}* cells. Thus, blockade of that residual autophagy by spautin-1 and *Atg5* siRNA upregulated senescence even further.

Interestingly, senescence induced by *Atg5* depletion was partially rescued by rapamycin in WT, but not in *ppargc1a^{-/-}* VSMCs cells. These data suggest that MTOR also regulates senescence by a mechanism different from its effect on autophagy. For instance, MTOR activates NFKB/NF- κ B (nuclear factor of kappa light polypeptide gene enhancer in B cells) [35], a major driver of the SASP [36]. We have demonstrated that activation of NFKB mediates the upregulation of NOX1 (NADPH oxidase 1) leading to increased ROS levels that promoted senescence of VSMCs [32]. Thus, inhibition of MTOR by rapamycin could also inhibit senescence by reducing oxidative stress. It is unknown, however, whether NADPH oxidases are upregulated by *Ppargc1a* deficiency. The fact that rapamycin was unable to rescue senescence induced by *Atg5* siRNA in *ppargc1a^{-/-}* cells could be related with the

higher levels of ROS in the knockout cells. Multiple sources of ROS can contribute to this elevated oxidative stress since PPARGC1A regulates the expression of several antioxidant enzymes, including SOD1, SOD2 and CAT, while regulating mitochondrial function. We demonstrated that downregulation of CAT increased ROS levels and senescence of VSMCs [28].

We hypothesized that SQSTM1 downregulation mediated the effect of *Ppargc1a* deficiency. In support of this hypothesis, we found that *sqstm1*^{-/-} cells mimicked the phenotype of *Ppargc1a* deficiency by presenting reduced proliferation, increased ROS levels, reduced LC3-II expression and autophagic flux and increased levels of NBR1 and senescence. In contrast to *ppargc1a*^{-/-}, *sqstm1*^{-/-} cells expressed higher levels of MTOR and its phosphorylated form, compared with WT cells. Further, *in vivo*, aortas of *sqstm1*^{-/-} mice showed more senescence and reduced levels of LC3-I.

Thus, altogether our data summarized in Figure 9 suggest that PPARGC1A upregulates autophagy by controlling the expression of SQSTM1 and that upregulation of mitochondrial biogenesis and autophagy reduces senescence of VSMCs. These findings are in part in line with previous observations in skeletal muscle. Brandt et al. recently showed that low and moderate intensity exercise training increased LC3-II:I ratio in WT, but not in *ppargc1a*^{-/-} mice [37]. However, only low-intensity exercise training showed reduced SQSTM1 levels in *ppargc1a*^{-/-} muscle. These observations suggest that PPARGC1A is required for the upregulation of autophagy in response to exercise in skeletal muscle; however, no differences in LC3-II:I ratio or in SQSTM1 levels were observed between untrained control WT and *ppargc1a*^{-/-} mice. In a skeletal muscle-specific *Ppargc1a* transgenic mouse, Halling et al. showed upregulated LC3-II:I ratio at rest and after exercise, compared with WT mice [38]. Interestingly,

SQSTM1 level was strongly downregulated in the transgenic animal, suggesting that the upregulation of autophagy caused SQSTM1 degradation. Further, Vainshtein et al. showed that exercise training upregulated *Sqstm1* mRNA levels in skeletal muscle of WT, but not in *ppargc1a*^{-/-} mice [39]. No difference at the mRNA level was observed in skeletal muscle of WT and *ppargc1a*^{-/-} mice in untrained control conditions [39]. In contrast to these studies, SQSTM1 protein and mRNA levels, as well as LC3 conversion, were significantly downregulated by *Ppargc1a* deficiency in VSMCs in our study. Although no difference in LC3-II:I ratio was observed in aortas of both genotypes *in vivo*, cargo containing autophagosome-like structures of various sizes were identified in VSMCs, as well as in the extracellular space of the media of the aorta. Accumulation of these structures suggests that the fusion with lysosomes and/or degradation in autolysosomes, but not the formation of autophagosomes, is inhibited in the absence of *Ppargc1a* *in vivo*. With respect to extracellular autophagosomes, it is possible that vesicle compartments containing autophagosome-like structures can fuse with the plasma membrane releasing autophagosomes into the extracellular media. In fact, autophagosomes can fuse with the plasma membrane under starvation conditions, a process that is regulated by the SNARE protein VAMP7 (vesicle-associated membrane protein 7) and is associated with the release of ATP [40]. Autophagosomes can also fuse with multivesicular bodies, organelles containing internal vesicles and exosomes, that fuse with the plasma membrane, releasing these vesicles into the extracellular media [41]. Furthermore, extracellular vesicles, including exosomes, can be secreted by senescent cells as part of the SASP [42]. Thus, increased accumulation of EM and the presence of extracellular vesicles in aortas of *ppargc1a*^{-/-} mice suggest that the SASP may contribute to tissue dysfunction *in vivo*. Whether

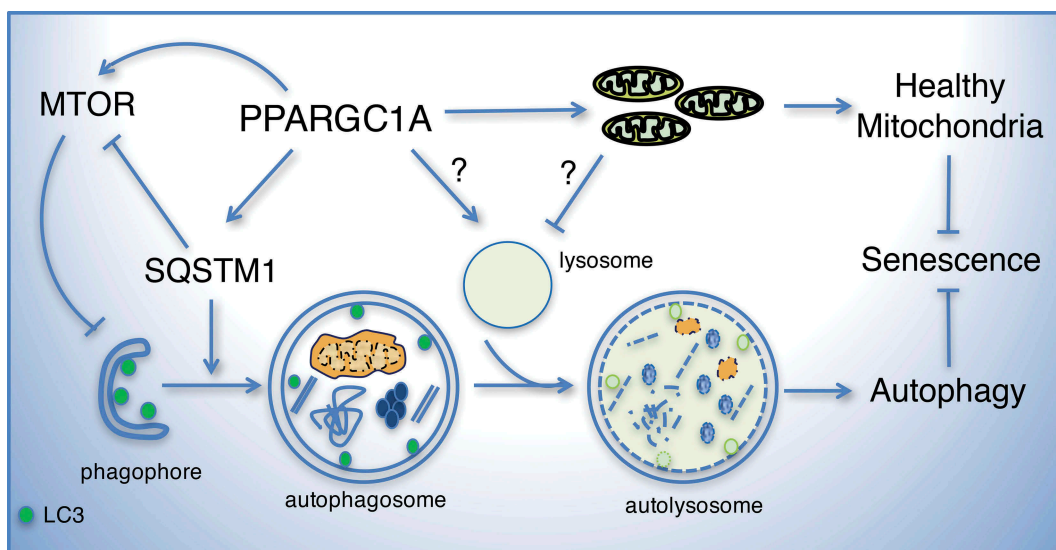


Figure 9. Model of the role of PPARGC1A and SQSTM1 in autophagy and senescence. Our data suggest that PPARGC1A regulates SQSTM1 expression leading to the upregulation of LC3-II and the stimulation of autophagy. Downregulation of PPARGC1A or SQSTM1 reduces LC3-II levels, autophagic flux, and cell proliferation and increases ROS levels and senescence. Elevated PPARGC1A expression or SQSTM1 deficiency increases MTOR phosphorylation creating a regulatory loop that may restrain excessive autophagy. It is unknown whether lysosomal dysfunction seen in PPARGC1A deficient cells also contributes to impaired autophagy. Altogether, the known functions of PPARGC1A, as a regulator of mitochondrial function and antioxidant capacity, together with its novel role, as a regulator of autophagy, contribute to reduced oxidative stress and senescence of VSMCs.

PPARGC1A regulates the secretion of extracellular vesicles remains to be elucidated.

In addition to the aorta tissue, SQSTM1 and LC3 expression was also downregulated in brain samples of *Ppargc1a*-deficient mice and in old compared with young C57BL/6 WT mice. TFRC and SOD2, two genes regulated by PPARGC1A in VSMCs, were also significantly reduced by the lack of *Ppargc1a* in the brain. Reduced protein expression of these genes during aging correlated with reduced mRNA levels. Brain samples from 1-year-old mice showed lower levels of *Sqstm1*, *Lc3* and *Ppargc1a* mRNA, compared with brains of 6-month-old animals. Interestingly, PPARGC1A is downregulated in postmortem brain samples of patients with Alzheimer disease and in neurons of the Tg2576 Alzheimer disease animal model [43]. Overexpression of PPARGC1A in these neurons reduced the formation of β -amyloid [43]. Our data suggest that secretion of autophagosomes and/or exosomes containing pathological aggregates, by reduced PPARGC1A expression, may contribute to the progression of Alzheimer disease. Thus, it is tempting to speculate that PPARGC1A could be protective to the brain, not only by maintaining mitochondrial function and the antioxidant capacity, but also by upregulating autophagy.

SQSTM1 protein expression was downregulated by *Ppargc1a* deficiency and upregulated by PPARGC1A overexpression, suggesting that SQSTM1 is a direct target of PPARGC1A; however, the molecular mechanism of this effect is unknown. *Sqstm1* transcription is regulated by NFE2L2 [44], a transcription factor co-activated by PPARGC1A [45], and by TFEB [14], a central regulator of lysosomal biogenesis [15]. The fact that *ppargc1a*^{-/-} VSMCs show reduced expression of the lysosomal proteins LAMP2 and CTSD and enlarged lysosomes suggests that TFEB may regulate both autophagy and lysosome biogenesis in VSMCs and that the function of TFEB may be altered by the absence of *Ppargc1a*. Interestingly, in SH-SY5Y neuroblastoma cells, overexpression of TFEB increased PPARGC1A expression leading to upregulation of mitochondrial biogenesis [46]. Similarly in skeletal muscle, exercise upregulated TFEB in a PPARGC1A-dependent manner [47], suggesting that TFEB and PPARGC1A can regulate each other. In this scenario, it is possible that upregulation of TFEB by PPARGC1A may upregulate autophagy by increasing SQSTM1 expression leading to LC3 conversion and may increase autophagic flux by increasing lysosome biogenesis, as suggested in our model (Figure 9). However, no changes in mRNA levels for lysosomal genes (*Lamp2* and *Ctsd*), or autophagy genes (*Lc3*, *Becn1* and *Nbr1*) were observed in *ppargc1a*^{-/-} cells. Only *Sqstm1* mRNA was significantly downregulated in these cells, suggesting that TFEB is likely not involved in this pathway.

ppargc1a^{-/-} cells also showed reduced expression of CTSD and LAMP2 and enlarged lysosomes, suggesting that lysosomal function may be impaired. Interestingly, treatment of both WT and *ppargc1a*^{-/-} cells with Chl, a drug that raises the pH of lysosomes [48], reduced CTSD protein levels. It is unknown whether changes in lysosome acidification may cause lysosomal dysfunction and/or reduced expression of CTSD and LAMP2 in cells lacking *Ppargc1a*. In fact, activation of the DNA damage response stimulates senescence [49]

and mediates the phosphorylation and inactivation of the vacuolar ATPase [50] leading to reduced lysosomal acidification. Increased DNA damage and telomere shortening were observed in *ppargc1a*^{-/-} VSMCs [7], suggesting that impaired function of the vacuolar ATPase could cause defective lysosomal function in these cells.

Lysosome dysfunction could be also caused by defective mitochondrial function, as suggested by Demers-Lamarche et al. Inhibition of mitochondrial function in this study resulted in impaired lysosome function and enlarged lysosomes [27]. It is also possible that reduced expression of lysosomal enzymes, like CTSD, can be caused by secretion of the enzyme. In fact, CTSD is secreted at low levels in physiologic conditions [51] and at high levels in cancer cells [52].

Autophagy is a protective process critically involved in VSMC function [53] that has been shown to reduce senescence of VSMCs [54,55] and to limit atherosclerosis [56]. We showed that inhibition of autophagy by 3-MA or spautin-1 induces senescence, while upregulation of autophagy by rapamycin reduces senescence induced by AGT II, a known inducer of cellular senescence in VSMCs [28,57]. However, overexpression of PPARGC1A significantly upregulated MTOR phosphorylation preventing LC3 conversion. In contrast, *Sqstm1* deficiency promoted a robust upregulation of MTOR. Thus, PPARGC1A and SQSTM1 seem to regulate a feedback loop mechanism, as shown in Figure 9, to maintain MTOR function and autophagy at physiological levels. This mechanism could be of importance to reduce autophagy and prevent autophagic cell death.

SQSTM1 is an autophagy receptor involved in the targeting of ubiquitinated proteins and organelles, like mitochondria, to autophagosomes for degradation. *sqstm1*^{-/-} mice have increased mitochondrial oxidative stress, decreased lifespan [17], mature-onset obesity and insulin resistance [18] and features of neurodegeneration [58]. Also, *Sqstm1* mutations are associated with Paget bone disease [59] and were also found in frontotemporal lobar degeneration and amyotrophic lateral sclerosis [60]. Here, we demonstrated that lack of *Sqstm1* is also associated with vascular senescence and that SQSTM1 downregulation mediates senescence caused by *Ppargc1a* deficiency. SQSTM1 downregulation by siRNA increased ROS levels, CDKN1A expression and SA-GLB1 activity basally and in response to AGT II and zinc overload, while SQSTM1 overexpression reduced ROS levels and SA-GLB1 activity in *ppargc1a*^{-/-} VSMCs. Also, overexpression of SQSTM1 upregulated LC3-II levels in WT and *ppargc1a*^{-/-} cells, suggesting that LC3 conversion is downstream of SQSTM1. Interestingly, lower levels of overexpressed SQSTM1 protein were observed in *ppargc1a*^{-/-} cells. Endogenous and overexpressed SQSTM1 accumulated at a similar level in *ppargc1a*^{-/-} cells treated with Chl (data not shown), suggesting that SQSTM1 is degraded by a lysosome-independent pathway.

Sqstm1 deficiency induces mature-onset obesity and insulin resistance at about 5 months of age [18]. Our observation that 2-month-old *sqstm1*^{-/-} male mice showed increased senescence in the aorta tissue suggests that senescence is not a consequence of the obesity phenotype of this animal model. Recently, increased atherosclerosis was also observed in

2-month-old *apoe*^{-/-}*sqstm1*^{-/-}, compared with *apoe*^{-/-} mice fed high fat diet [19]. It is unknown, however, whether accelerated aging by the lack of *Sqstm1* promotes atherosclerosis. It is also unknown whether the molecular mechanism involved in *Sqstm1* deficiency-induced senescence depends mainly on the inhibition of autophagy. Since SQSTM1 overexpression reduces ROS levels in *ppargc1a*^{-/-} VSMCs and *sqstm1*^{-/-} cells showed increased ROS levels, it is likely that other mechanisms are also involved.

Telomere dysfunction causes mitochondrial dysfunction by a TRP53-dependent downregulation of PPARGC1A and PPARGC1B leading to mitochondrial dysfunction and increased ROS production [61]. This evidence supports a unified view of aging in which DNA damage to telomeres induces metabolic and mitochondrial compromise leading to accelerated aging [62,63]. PPARGC1A is central to this regulatory network [64] by regulating mitochondrial function, the expression of antioxidant enzymes, and as shown here, autophagy.

Altogether, our data demonstrate that senescence induced by *Ppargc1a* deficiency is mediated by impaired autophagy caused by SQSTM1 downregulation. The phenotype of *sqstm1*^{-/-} and *ppargc1a*^{-/-} mice is similar in terms of accelerated vascular aging and atherosclerosis. Our data also suggest that measurements of SQSTM1 protein expression, as an indicator of successful autophagy, should be evaluated carefully since in our study reduced SQSTM1 expression was associated with defective autophagy, but not with upregulation of autophagic flux.

Materials and methods

Antibodies and reagents

Rabbit antibodies against LC3 (2765), BECN1 (3738), phosphorylated MTOR (Ser2448, 2971) and MTOR (2983) were from Cell Signaling Technology. Goat anti-CTSD (C-20, sc-6486), and rabbit anti-SQSTM1 (H290, sc-25575) and anti-CDKN1A (sc397) were from Santa Cruz Biotechnology. Rabbit antibodies against LAMP2 (L0668), CAT (219010) and ATG5 (A0856), and mouse antibodies against TUBG1 (T5326), ACTB (A5441), and ACTA2 (A5228) were from Sigma-Aldrich. Mouse TRP53 (BML-SA293-0050) and rabbit SOD2 (ADI-SOD-110) antibodies were from Enzo Life Science. Mouse TFRC antibody was from Invitrogen (136800). Rabbit CTSD (ab75852) and mouse SQSTM1 (ab56416) and NBR1 (ab55474) antibodies were from Abcam. Mouse (MA5-15738) and rabbit (PA1-988) GAPDH (glyceraldehyde-3-phosphate dehydrogenase) antibodies were from Thermo Fisher Scientific. PPARGC1A antibody was from Dr. D. Kelly (Perelman School of Medicine, University of Pennsylvania), as described previously [33].

AGT II (A6402), 3-MA (M9281), Chl (C6628), rapamycin (553210), spautin-1 (SML0440-5MG) and protease inhibitor cocktail (P340-5ML) were from Sigma-Aldrich. Fetal bovine serum (FBS, 97,068-075) was from Seradigm. 2',7'-dichlorodihydrofluorescein diacetate (H₂DCFDA, C6827) and dihydroethidium (DHE, D11347) were from Invitrogen. Fluorescein-di-β-D-galactopyranoside (FDG, MO250) was from Marker Gene Technologies. Collagenase type 2 (LS004204) and elastase (LS006363) were from Worthington

Biochemical Corporation. Adenovirus containing PPARGC1A was obtained from Dr. Wayne Alexander at Emory University [33]. Adenovirus containing HA-tagged human SQSTM1 (4 x 10¹⁰ plaque-forming units [PFU]/ml) was from Vector Biolabs.

Mice

Animal experiments using *Ppargc1a*^{+/+} and *ppargc1a*^{-/-} (obtained from Dr. Wayne Alexander at Emory University [6]) and *sqstm1*^{-/-} mice in the C57BL/6 background (obtained from Dr. Toru Yanagawa at the University of Tsukuba, Japan [65]) were performed in compliance with the Institutional Animal Care and Use Committee of Emory University and Florida State University, respectively. Animals were euthanized using CO₂ and aortas were isolated for measurements of protein expression or for isolation of VSMCs.

Isolation of vsmcs, cell culture and adenovirus transduction

RASMs were isolated by enzymatic digestion as previously described [66]. Briefly, aortas from 5 male Sprague-Dawley rats (2-month-old) were cleaned from periadventitial fat, washed in Hanks balanced salt buffer (Corning, 21-021-CV) and digested with 175 units/ml collagenase for 30 min at 37°C to remove the adventitial layer. The endothelium was removed using a sterile cotton swab and aortas were incubated in DMEM (Corning, 10-014-CV) overnight, and then digested with 175 units/ml collagenase and 0.5 mg/ml elastase for 1 h at 37°C. VSMCs released after digestion were centrifuged and cell pellets resuspended in DMEM media. Isolation of MASMs was performed using a similar protocol, with the exception that after collagenase digestion and overnight incubation, aortas were cut into small pieces, which were allowed to attach to culture plates for at least 3 d. Both RASMs and MASMs were cultured in DMEM containing 1 g/L glucose, 100 U/ml penicillin, 100 mg/ml streptomycin, 2 mM glutamine (Corning, 30-009-CI) and 10% FBS at 37°C in a 5% CO₂ incubator. Contamination of cell cultures with fibroblasts was assessed by immunofluorescence using fibroblast antigen antibodies, as shown in Fig. S4. Cells were used for experiments between passages 4 and 12, as we previously reported [6,28,34]. For AGT II and zinc treatment, cells were starved in DMEM containing 0.5% FBS for 24 h and then incubated in the same media with 100 nM AGT II or 50 μM zinc (Sigma-Aldrich, Z0251) for 3 d, as previously described [67]. Cells were treated with 50 μM Chl, 10 mM 3-MA, 100 nM rapamycin or 10 μM spautin-1 in DMEM 0.5% FBS.

For adenovirus infection, cells were incubated with adenovirus containing *PPARGC1A* (Ad.PGC1A), *SQSTM1* (Ad.SQSTM1) or empty adenovirus for 1 h in plain DMEM medium. Cells were allowed to recover in complete medium for 48 h prior to experimental treatment.

Transmission electron microscopy (TEM)

Immediately after CO₂ euthanasia, mice were perfused from the left ventricle and aortas prepared for TEM analysis, as

previously reported [68]. Aorta samples were fixed overnight in 2.5% glutaraldehyde (Electron Microscopy Sciences, 111-30-8) in 0.1 M sodium cacodylate (Electron Microscopy Sciences, 12300) buffer, followed by postfixation in 1% osmium tetroxide (Electron Microscopy Sciences, 19112) in 0.1 M sodium cacodylate buffer, dehydration in a graded ethanol series followed by propylene oxide (Electron Microscopy Sciences, 20410), and embedding in Epon-812 resin (Sigma-Aldrich, 45345). Semi-thin transverse sections were stained with 0.5% aqueous Toluidine Blue O (Sigma-Aldrich, 89640) and brightfield images were taken with a Zeiss Axioskop equipped with an RT Slider Spot Camera. Ultrathin, transverse sections were poststained with uranyl acetate and lead citrate. Images were taken on a Hitachi H-7500 electron microscope operated at 75 kV in the Robert P. Apkarian Integrated Electron Microscopy Core at Emory University. The images were imported into Image-Pro Plus v. 6.2 software (MediaCybernetics, 41N51000-LUSB) for morphometric area measurements of EM.

Morphometric measurements

Area measurements of aortic images were performed using Image-Pro Plus 6.2 software. First, using the Measurements/ Create Polygon feature of the software, total area between two elastin lamellae (total interlamellar area) was traced and was measured. Within these interlamellar zones, fibrillar/amorphous areas of EM were also measured. These area measurements were expressed in μm^2 . The EM areas were divided by the total medial layer area and expressed as % EM in the medial layers.

Senescence associated GLB1/ β -galactosidase (SA-GLB1) staining

SA-GLB1 activity was determined as previously described [34]. Cells were washed with PBS (Corning, 21-40-CV) and then fixed with 0.2% glutaraldehyde in PBS for 10 min at room temperature. After fixation, cells were washed with PBS and were incubated overnight at 37°C in 40 mM phosphate buffer (4.8 mM Na_2HPO_4 , 35.2 NaH_2PO_4 , pH 6.0) supplemented with 1 mg/ml X-Gal (Amresco, X1205), 2 mM MgCl_2 , 150 mM NaCl, 5 mM $\text{K}_4\text{Fe}(\text{CN})_6$ (Sigma-Aldrich, P3289) and 5 mM $\text{K}_3\text{Fe}(\text{CN})_6$ (Sigma-Aldrich, P8131). Images were taken using an Axio Observer.A1 microscope (Carl Zeiss) using a 10 \times objective. SA-GLB1-positive cells were expressed as a percentage of total cell number. In addition, FDG (Ex/Em: 485/515 nm), a fluorescent analog of X-gal, was used to measure SA-GLB1 using a Synergy H1 multi-mode plate reader (BioTek Instruments).

Immunofluorescence

Immunofluorescence was performed in cells fixed with 4% paraformaldehyde (PFA) (Sigma-Aldrich, P6148), as previously described [69]. Coverslips were washed with PBS and permeabilized in buffer containing 2% BSA (Sigma-Aldrich, A7906), 1% fish skin gelatin (Sigma-Aldrich, G7041), 0.02% saponin (Sigma-Aldrich, S4521) and 15% horse serum (Corning, 35-030-CV) in PBS. Secondary

antibodies included Alexa Fluor[®] 568 and Alexa Fluor[®] 488 (Molecular Probes). 4',6'-diamidino-2-phenylindole (DAPI) (Biotium, 40,011) was used to stain the nuclei. Images were acquired using the 488- and 543-nm lines of the argon ion as well as green HeNe lasers with 515/30-nm band pass and 585-nm-long pass filters, respectively, in a confocal imaging system (Zeiss LSM 510 META) in the Department of Medicine at Emory University. Quantification of LC3 and SQSTM1 puncta was performed using ImageJ software (NIH). Briefly, each cell was traced, and the image was converted into an 8-bit grayscale. Then, using the edit/clear outside feature of the software, background was removed and the image was inverted to quantify puncta as black dots. A threshold was then applied, the size of the particles to be quantified was set and the number of puncta was determined using the analyzed particle feature of the software.

Reactive oxygen species measurements

ROS levels were measured using H_2DCFDA and DHE, which were described previously [34]. Cells were washed once with DPBS (Dulbecco's phosphate-buffered saline, Corning, 21-030-CV) and incubated with 10 μM H_2DCFDA or DHE in DPBS for 30 min at 37°C. Fluorescence intensity for DHE (Ex/Em: 500/530 nm) and for H_2DCFDA (Ex/Em: 492/520 nm) was determined using a Synergy H1 multi-mode plate reader (BioTek Instruments).

Western blotting

VSMCs were lysed in buffer A (50 mM HEPES, pH 7.4, 150 mM NaCl, 1 mM EGTA, 0.1 mM MgCl_2) supplemented with 1% Triton X-100 (Sigma-Aldrich, X100-500ML), 2 mM sodium orthovanadate (Enzo Life Sciences, 400-032-G025), 10 mM sodium pyrophosphate (Sigma-Aldrich, 221368), 10 mM sodium fluoride (J. T. Baker, 3688-01), and protease cocktail inhibitor for 30 min on ice. Aortas were homogenized with 15 strokes of a Teflon/glass homogenizer in buffer A. Cell extracts were sonicated and equal amounts of protein from total extracts were separated using 10% SDS-PAGE gels or 4–20% Criterion precast gels (Bio-Rad, 5671094). Gels were transferred to PVDF (Thermo Scientific, PI88518) membranes and blocked for 20 min with 1% non-fat dry milk (Bio-Rad, 170-6404) in TBS buffer (150 mM NaCl, 50 mM Tris-HCl, pH 7.4) supplemented with 0.05% Triton X-100 (TBS-T). Membranes were incubated with primary antibodies in PBS containing 3% BSA, washed 3 times with TBS-T 10 min each and incubated with HRP-conjugated secondary antibodies (Invitrogen, G-21234 [goat anti rabbit], R-21459 [rabbit anti goat], G-21040 [goat anti mouse]). After 3 washes with TBS-T, membranes were developed by enhanced chemiluminescence. Quantification of bands in western blots, including loading controls, within the linear range was performed using ImageJ software.

Reverse transcription PCR (RT-PCR) and RNA interference

Total RNA was extracted using the RNeasy kit (Qiagen, 74104) according to the manufacturer's instructions. The SuperScript[™] One Step RT-PCR system (Invitrogen, 109280) was used to

measure the mRNA levels of *Pparg1a*, *Pparg1b*, *Sqstm1*, *Nbr1*, *Becn1*, *Optn*, *Ctsd*, *Lamp2*, *Lc3* and *Gapdh*. Oligonucleotides, listed in Table S1, were obtained from Sigma-Aldrich.

Downregulation of rat *Sqstm1* in RASM cells was achieved using the following siRNA duplex from Invitrogen: CGGUGAAGGCCUAUCUACUGGGCAA and UUGCCCAGUAGAUAGGCCUUCACCG. Cells were transfected using the basic Nucleofector® kit for smooth muscle cells from Amaxa Biosystems. Downregulation of mouse *Atg5* in MASMs was done using siRNAControl#1 and *siAtg5* from Thermo Fisher Scientific (GGUUAUGAGACAAGAAGAUtt and AUCUU CUUGUCUCAUAACCTt).

Cell proliferation

Pparg1a^{+/+} and *Pparg1a*^{-/-} MASMs (5,000 cells/per well) were grown in complete media at 37°C for 2 d. Cells were starved for 48 h in DMEM supplemented with 0.5% FBS and then incubated in complete media with 10% FBS and counted every day for 4 d.

Statistical analysis

Data were analyzed by student's T-test and one-way analysis of variance (ANOVA). Values were expressed as mean ± standard deviation (SD). $p \leq 0.05$ was considered as statistically significant. For western blots, protein expression was adjusted by the level of loading controls (TUBG1, GAPDH or ACTB) in at least 3 independent experiments.

Acknowledgments

We thank Dr. Wayne Alexander at the Department of Medicine Emory University for his support. The content is solely the responsibility of the authors and does not necessarily reflect the official views of the National Institutes of Health.

Disclosure statement

No potential conflict of interest was reported by the authors.

Funding

This work was supported in part by the American Federation for Aging Research, the American Heart Association (14GRNT20180028), the USDA (2018-67017-27518) and the Robert P. Apkarian Integrated Electron Microscopy Core (RPAIEMC), which is subsidized by the Emory College of Arts and Sciences and the Emory University School of Medicine and is one of the Emory Integrated Core Facilities. Additional support was provided by the National Center for Advancing Translational Sciences of the National Institutes of Health under award number UL1TR000454 and from the National Institute of Health award numbers UO1 HL80711 and HL60728 of Dr. Wayne Alexander.

ORCID

Nikolay Patrushev  <http://orcid.org/0000-0002-0837-5259>

References

- [1] Hubbard VM, Valdor R, Macian F, et al. Selective autophagy in the maintenance of cellular homeostasis in aging organisms. *BioGerontology*. 2012;13(1):21–35.
- [2] Cuervo AM, Dice JF. Age-related decline in chaperone-mediated autophagy. *J Biol Chem*. 2000;275(40):31505–31513.
- [3] Zahn JM, Sonu R, Vogel H, et al. Transcriptional profiling of aging in human muscle reveals a common aging signature. *PLoS Genet*. 2006;2(7):e115.
- [4] Vina J, Gomez-Cabrera MC, Borrás C, et al. Mitochondrial biogenesis in exercise and in ageing. *Adv Drug Deliv Rev*. 2009;61(14):1369–1374.
- [5] Handschin C, Spiegelman BM. Peroxisome proliferator-activated receptor gamma coactivator 1 coactivators, energy homeostasis, and metabolism. *Endocr Rev*. 2006;27(7):728–735.
- [6] Xiong S, Salazar G, Patrushev N, et al. Peroxisome proliferator-activated receptor gamma coactivator-1alpha is a central negative regulator of vascular senescence. *Arterioscler Thromb Vasc Biol*. 2013;33(5):988–998.
- [7] Xiong S, Patrushev N, Forouzanmehr F, et al. PGC-1alpha modulates telomere function and DNA damage in protecting against aging-related chronic diseases. *Cell Rep*. 2015;12(9):1391–1399.
- [8] Lemasters JJ. Selective mitochondrial autophagy, or mitophagy, as a targeted defense against oxidative stress, mitochondrial dysfunction, and aging. *Rejuvenation Res*. 2005;8(1):3–5.
- [9] Klionsky DJ, Emr SD. Autophagy as a regulated pathway of cellular degradation. *Science*. 2000;290(5497):1717–1721.
- [10] Kang HT, Lee KB, Kim SY, et al. Autophagy impairment induces premature senescence in primary human fibroblasts. *PLoS One*. 2011;6(8):e23367.
- [11] Tai H, Wang Z, Gong H, et al. Autophagy impairment with lysosomal and mitochondrial dysfunction is an important characteristic of oxidative stress-induced senescence. *Autophagy*. 2017;13(1):99–113.
- [12] Grootaert MO, Da Costa Martins PA, Bitsch N, et al. Defective autophagy in vascular smooth muscle cells accelerates senescence and promotes neointima formation and atherogenesis. *Autophagy*. 2015;11(11):2014–2032.
- [13] Geisler S, Holmström KM, Skujat D, et al. PINK1/Parkin-mediated mitophagy is dependent on VDAC1 and p62/SQSTM1. *Nat Cell Biol*. 2010;12(2):119–131.
- [14] Settembre C, Di Malta C, Polito VA, et al. TFEB links autophagy to lysosomal biogenesis. *Science*. 2011;332(6036):1429–1433.
- [15] Sardiello M, Palmieri M, Di Ronza A, et al. A gene network regulating lysosomal biogenesis and function. *Science*. 2009;325(5939):473–477.
- [16] Scott I, Webster BR, Chan CK, et al. GCN5-like protein 1 (GCN5L1) controls mitochondrial content through coordinated regulation of mitochondrial biogenesis and mitophagy. *J Biol Chem*. 2014;289(5):2864–2872.
- [17] Kwon J, Han E, Bui C-B, et al. Assurance of mitochondrial integrity and mammalian longevity by the p62-Keap1-Nrf2-Nqo1 cascade. *EMBO Rep*. 2012;13(2):150–156.
- [18] Rodriguez A, Durán A, Selloum M, et al. Mature-onset obesity and insulin resistance in mice deficient in the signaling adapter p62. *Cell Metab*. 2006;3(3):211–222.
- [19] Sergin I, Bhattacharya S, Emanuel R, et al. Inclusion bodies enriched for p62 and polyubiquitinated proteins in macrophages protect against atherosclerosis. *Sci Signal*. 2016;9(409):ra2–ra2.
- [20] Pugsley HR. Assessing autophagic flux by measuring LC3, p62, and LAMP1 Co-localization using multispectral imaging flow cytometry. *J Vis Exp*. 2017 125.
- [21] O'Hagan KA, Cocchiglia S, Zhdanov AV, et al. PGC-1alpha is coupled to HIF-1alpha-dependent gene expression by increasing mitochondrial oxygen consumption in skeletal muscle cells. *Proc Natl Acad Sci U S A*. 2009;106(7):2188–2193.
- [22] Rensvold JW, Ong S-E, Jeevananthan A, et al. Complementary RNA and protein profiling identifies iron as a key regulator of mitochondrial biogenesis. *Cell Rep*. 2013;3(1):237–245.

- [23] Mellone M, Hanley CJ, Thirdborough S, et al. Induction of fibroblast senescence generates a non-fibrogenic myofibroblast phenotype that differentially impacts on cancer prognosis. *Aging* (Albany NY). 2016;9(1):114–132.
- [24] Liu CL, Chen S, Dietrich D, et al. Changes in autophagy after traumatic brain injury. *J Cereb Blood Flow Metab*. 2008;28(4):674–683.
- [25] Viscomi MT, D'Amelio M, Cavallucci V, et al. Stimulation of autophagy by rapamycin protects neurons from remote degeneration after acute focal brain damage. *Autophagy*. 2012;8(2):222–235.
- [26] Nikolettou V, Sidiropoulou K, Kallergi E, et al. Modulation of autophagy by BDNF underlies synaptic plasticity. *Cell Metab*. 2017;26(1):230–242 e5.
- [27] Demers-Lamarche J, Guillebaud G, Tlili M, et al. Loss of mitochondrial function impairs lysosomes. *J Biol Chem*. 2016;291(19):10263–10276.
- [28] Patrushev N, Seidel-Rogol B, Salazar G. Angiotensin II requires zinc and downregulation of the zinc transporters ZnT3 and ZnT10 to induce senescence of vascular smooth muscle cells. *PLoS One*. 2012;7(3):e33211.
- [29] Wu YT, Tan H-L, Shui G, et al. Dual role of 3-methyladenine in modulation of autophagy via different temporal patterns of inhibition on class I and III phosphoinositide 3-kinase. *J Biol Chem*. 2010;285(14):10850–10861.
- [30] Liu J, Xia H, Kim M, et al. Beclin1 controls the levels of p53 by regulating the deubiquitination activity of USP10 and USP13. *Cell*. 2011;147(1):223–234.
- [31] Nazio F, Strappazzon F, Antonioli M, et al. mTOR inhibits autophagy by controlling ULK1 ubiquitylation, self-association and function through AMBRA1 and TRAF6. *Nat Cell Biol*. 2013;15(4):406–416.
- [32] Salazar G, Huang J, Feresin RG, et al. Zinc regulates Nox1 expression through a NF-kappaB and mitochondrial ROS dependent mechanism to induce senescence of vascular smooth muscle cells. *Free Radic Biol Med*. 2017;108:225–235.
- [33] Xiong S, Salazar G, San Martin A, et al. PGC-1 alpha serine 570 phosphorylation and GCN5-mediated acetylation by angiotensin II drive catalase down-regulation and vascular hypertrophy. *J Biol Chem*. 2010;285(4):2474–2487.
- [34] Feresin RG, Huang J, Klarich DS, et al. Blackberry, raspberry and black raspberry polyphenol extracts attenuate angiotensin II-induced senescence in vascular smooth muscle cells. *Food Funct*. 2016;7(10):4175–4187.
- [35] Dan HC, Cooper MJ, Cogswell PC, et al. Akt-dependent regulation of NF- κ B is controlled by mTOR and Raptor in association with IKK. *Genes Dev*. 2008;22(11):1490–1500.
- [36] Chien Y, Scuoppo C, Wang X, et al. Control of the senescence-associated secretory phenotype by NF-kappaB promotes senescence and enhances chemosensitivity. *Genes Dev*. 2011;25(20):2125–2136.
- [37] Brandt N, Dethlefsen MM, Bangsbo J, et al. PGC-1alpha and exercise intensity dependent adaptations in mouse skeletal muscle. *PLoS One*. 2017;12(10):e0185993.
- [38] Halling JF, Ringholm S, Nielsen MM, et al. PGC-1alpha promotes exercise-induced autophagy in mouse skeletal muscle. *Physiol Rep*. 2016;4(3).
- [39] Vainshtein A, Tryon LD, Pauly M, et al. Role of PGC-1alpha during acute exercise-induced autophagy and mitophagy in skeletal muscle. *Am J Physiol Cell Physiol*. 2015;308(9):C710–9.
- [40] Fader CM, Aguilera MO, Colombo MI. ATP is released from autophagic vesicles to the extracellular space in a VAMP7-dependent manner. *Autophagy*. 2012;8(12):1741–1756.
- [41] Fader CM, Sánchez DG, Mestre MB, et al. TI-VAMP/VAMP7 and VAMP3/cellubrevin: two v-SNARE proteins involved in specific steps of the autophagy/multivesicular body pathways. *Biochim Biophys Acta*. 2009;1793(12):1901–1916.
- [42] Kadota T, Fujita Y, Yoshioka Y, et al. Emerging role of extracellular vesicles as a senescence-associated secretory phenotype: Insights into the pathophysiology of lung diseases. *Mol Aspects Med*. 2018;60:92–103.
- [43] Qin W, Haroutunian V, Katsel P, et al. PGC-1alpha expression decreases in the Alzheimer disease brain as a function of dementia. *Arch Neurol*. 2009;66(3):352–361.
- [44] Jain A, Lamark T, Sjøttem E, et al. p62/SQSTM1 is a target gene for transcription factor NRF2 and creates a positive feedback loop by inducing antioxidant response element-driven gene transcription. *J Biol Chem*. 2010;285(29):22576–22591.
- [45] Gleyzer N, Vercauteren K, Scarpulla RC. Control of mitochondrial transcription specificity factors (TFB1M and TFB2M) by nuclear respiratory factors (NRF-1 and NRF-2) and PGC-1 family coactivators. *Mol Cell Biol*. 2005;25(4):1354–1366.
- [46] Ivankovic D, Chau K-Y, Schapira AHV, et al. Mitochondrial and lysosomal biogenesis are activated following PINK1/parkin-mediated mitophagy. *J Neurochem*. 2016;136(2):388–402.
- [47] Erlich AT, Brownlee DM, Beyfuss K, et al. Exercise induces TFEB expression and activity in skeletal muscle in a PGC-1alpha-dependent manner. *Am J Physiol Cell Physiol*. 2018;314(1):C62–C72.
- [48] Seglen PO, Gordon PB. Effects of lysosomotropic monoamines, diamines, amino alcohols, and other amino compounds on protein degradation and protein synthesis in isolated rat hepatocytes. *Mol Pharmacol*. 1980;18(3):468–475.
- [49] Freund A, Patil CK, Campisi J. p38MAPK is a novel DNA damage response-independent regulator of the senescence-associated secretory phenotype. *Embo J*. 2011;30(8):1536–1548.
- [50] Kang HT, Park JT, Choi K, et al. Chemical screening identifies ATM as a target for alleviating senescence. *Nat Chem Biol*. 2017;13(6):616–623.
- [51] Zuhlsdorf M, Imort M, Hasilik A, et al. Molecular forms of beta-hexosaminidase and cathepsin D in serum and urine of healthy subjects and patients with elevated activity of lysosomal enzymes. *Biochem J*. 1983;213(3):733–740.
- [52] Dubey V, Luqman S. Cathepsin D as a promising target for the discovery of novel anticancer agents. *Curr Cancer Drug Targets*. 2017;17(5):404–422.
- [53] Tai S, Hu X-Q, Peng D-Q, et al. The roles of autophagy in vascular smooth muscle cells. *Int J Cardiol*. 2016;211:1–6.
- [54] Luo Z, Xu W, Ma S, et al. Moderate autophagy inhibits vascular smooth muscle cell senescence to stabilize progressed atherosclerotic plaque via the mTORC1/ULK1/ATG13 signal pathway. *Oxid Med Cell Longev*. 2017;2017:3018190.
- [55] Sung JY, Lee KY, Kim JR, et al. Interaction between mTOR pathway inhibition and autophagy induction attenuates adriamycin-induced vascular smooth muscle cell senescence through decreased expressions of p53/p21/p16. *Exp Gerontol*. 2017;109:51–58.
- [56] Grootaert MOJ, Moulis M, Roth L, et al. Vascular smooth muscle cell death, autophagy and senescence in atherosclerosis. *Cardiovasc Res*. 2018;114(4):622–634.
- [57] Kunieda T, Minamino T, Nishi J-I, et al. Angiotensin II induces premature senescence of vascular smooth muscle cells and accelerates the development of atherosclerosis via a p21-dependent pathway. *Circulation*. 2006;114(9):953–960.
- [58] Ramesh Babu J, Lamar Seibenhener M, Peng J, et al. Genetic inactivation of p62 leads to accumulation of hyperphosphorylated tau and neurodegeneration. *J Neurochem*. 2008;106(1):107–120.
- [59] Laurin N, Brown JP, Morissette J, et al. Recurrent mutation of the gene encoding sequestosome 1 (SQSTM1/p62) in Paget disease of bone. *Am J Hum Genet*. 2002;70(6):1582–1588.
- [60] Rubino E, Rainero I, Chiò A, et al. SQSTM1 mutations in frontotemporal lobar degeneration and amyotrophic lateral sclerosis. *Neurology*. 2012;79(15):1556–1562.
- [61] Sahin E, Colla S, Liesa M, et al. Telomere dysfunction induces metabolic and mitochondrial compromise. *Nature*. 2011;470(7334):359–365.
- [62] Kelly DP. Cell biology: Ageing theories unified. *Nature*. 2011;470(7334):342–343.
- [63] Sahin E, DePinho RA. Axis of ageing: telomeres, p53 and mitochondria. *Nat Rev Mol Cell Biol*. 2012;13(6):397–404.
- [64] Salazar G. NADPH oxidases and mitochondria in vascular senescence. *Int J Mol Sci*. 2018;19(5):1325.

- [65] Komatsu M, Waguri S, Koike M, et al. Homeostatic levels of p62 control cytoplasmic inclusion body formation in autophagy-deficient mice. *Cell*. 2007;131(6):1149–1163.
- [66] Griending KK, Taubman MB, Akers M, et al. Characterization of phosphatidylinositol-specific phospholipase C from cultured vascular smooth muscle cells. *J Biol Chem*. 1991;266(23):15498–15504.
- [67] Feresin RG, Pourafshar S, Huang J, et al. Extraction and purification of polyphenols from freeze-dried berry powder for the treatment of vascular smooth muscle cells in vitro. *JoVE*. 2017;125:e55605.
- [68] Sutliff RL, Hilenski LL, Amanso AM, et al. Polymerase delta interacting protein 2 sustains vascular structure and function. *Arterioscler Thromb Vasc Biol*. 2013;33(9):2154–2161.
- [69] Zhao Y, Feresin RG, Falcon-Perez JM, et al. Differential targeting of SLC30A10/ZnT10 heterodimers to endolysosomal compartments modulates EGF-induced MEK/ERK1/2 activity. *Traffic*. 2016;17(3):267–288.